Chemical Geology 273 (2010) 8–34

Contents lists available at ScienceDirect

Chemical Geology

journal homepage: www.elsevier.com/locate/chemgeo

In situ U–Pb, Sr, Nd and Hf isotopic analysis of eudialyte by LA-(MC)-ICP-MS

Fu-Yuan Wu [a,*], Yue-Heng Yang [a], Michael A.W. Marks [b], Zhi-Chao Liu [a], Qin Zhou [a], Wen-Chun Ge [c], Jing-Sui Yang [d], Zi-Fu Zhao [e], Roger H. Mitchell [f], Gregor Markl [b]

[a] State Key Laboratory of Lithospheric Evolution, Institute of Geology and Geophysics, Chinese Academy of Sciences, P. O. Box 9825, Beijing 100029, China
[b] Institut für Geowissenschaften, Eberhard–Karls–Universität Tübingen, Wilhelmstrasse 56, D–72074 Tübingen, Germany
[c] College of Earth Sciences, Jilin University, Changchun 130061, China
[d] Institute of Geology, Chinese Academy of Geological Sciences, Beijing 100037, China
[e] CAS Key Laboratory of Crust-Mantle Materials and Environments, School of Earth and Space Science, University of Science and Technology of China, Hefei 230026, China
[f] Department of Geology, Lakehead University, Thunder Bay, Ontario, Canada P7B 5E1

ARTICLE INFO

Article history:
Received 15 August 2009
Received in revised form 4 February 2010
Accepted 4 February 2010

Editor: R.L. Rudnick

Keywords:
U–Pb ages
Sr, Nd and Hf isotopic ratios
Eudialyte
Laser ablation
Agpaitic syenites

ABSTRACT

Eudialytes are a group of complex Na–Ca zirconosilicate minerals that generally occur in peralkaline agpaitic syenites. Given that eudialytes are easily altered and commonly contain inclusions of earlier-crystallized minerals, *in situ* laser ablation is considered as the most suitable method to determine their U–Pb ages, and Sr, Nd and Hf isotopic compositions. Electron microprobe and LA-ICP-MS analysis of eudialytes from nepheline syenites from Ilímaussaq (Greenland), Khibiny and Lovozero (Russia), Saima (China), Tamazeght (Morocco), Kipawa and Mont Saint Hilaire (Canada), Poços de Caldas (Brazil) and Langesund Fjord (Norway), indicate that this mineral typically has high contents of U, Pb, Nb, Ta, Zr, Hf and rare earth elements (REE).

Analysis of an in-house standard eudialyte by both solution and laser ablation methods demonstrates that precise and accurate U–Pb ages can be obtained from eudialyte after correction for the common Pb content. The high Sr, Nd and Hf contents in eudialyte, coupled with the generally low Rb/Sr and Lu/Hf ratios, also permit the precise determination of *in situ* Sr, Nd and Hf isotopic ratios by LA-(MC)-ICP-MS methods. However, some eudialytes with Rb/Sr ratio of >0.02 and Yb/Sr>0.1, and Lu/Hf>0.08 (or Yb/Hf>0.4–0.5) cannot be used for *in situ* Sr and Hf isotopic measurement. Eudialyte is the only mineral investigated to date for which it is possible to determine simultaneously U–Pb ages and Sr, Nd and Hf isotopic compositions.

1. Introduction

Sr, Nd and Hf isotopic data are essential for deciphering the petrogenesis of rocks. A common procedure utilized in the past was to obtain data by bulk rock elemental and isotopic analysis, and from these data determine the initial isotopic compositions. Problems with this approach are that samples are commonly contaminated by crustal and/or xenolithic material and thus the isotopic ratios determined do not represent those of the parental magma. To avoid such problems laser ablation multi-collector inductively coupled plasma mass spectrometry (LA-MC-ICP-MS), has been extensively used for *in situ* isotopic measurements as it can provide rapid, texturally sensitive, high precision isotopic data without the need for chemical preparation of the samples. For Sr isotopic analysis, *in situ* laser ablation techniques have been applied minerals with low Rb/Sr ratios, i.e., plagioclase, titanite, apatite and perovskite (Christensen et al., 1995; Ramos et al., 2004; Adams et al., 2005; Woodhead et al., 2005; Davidson et al., 2007; Paton et al., 2007a,b; Yang et al., 2009). With regard to Nd, this technique has been recently applied to minerals with high Nd concentrations such as: apatite, titanite, monazite, allanite, and perovskite (Foster and Vance, 2006; McFarlane and McCulloch, 2007, 2008; Yang et al., 2008; Gregory et al., 2009; Wu et al., 2010; Yang et al., 2009). Hf isotopic analyses have been obtained for zircon, baddeleyite and rutile (Thirlwall and Walder, 1995; Griffin et al., 2000; Choukroun et al., 2005; Wu et al., 2006; Aulbach et al., 2008), as these minerals have high Hf concentrations and low Lu/Hf ratios.

Commonly, it is not possible to obtain Sr, Nd and Hf isotopic data from a single mineral phase. The ideal candidate has to have high Sr, Nd and Hf concentrations, coupled with low Rb/Sr and Lu/Hf ratios. Eudialyte group minerals have great potential for such multiple isotopic ratio determinations as recently shown by Kogarko et al. (2010).

On the basis of mineralogical differences and peralkalinity [molar (Na + K)/Al>1], igneous rocks are subdivided into miaskitic and agpaitic groups (Johnsen and Gault, 1997; Sørensen, 1997). In miaskitic rocks, zircon, baddeleyite, titanite, ilmenite and rutile are common; whereas in agpaitic rocks, complex Na–Ca zirconosilicates

* Corresponding author. Tel.: +86 10 82998217; fax: +86 10 62010846.
E-mail address: wufuyuan@mail.igcas.ac.cn (F.-Y. Wu).

0009-2541/$ – see front matter © 2010 Elsevier B.V. All rights reserved.
doi:10.1016/j.chemgeo.2010.02.007

such as eudialyte, rinkite and låvenite are present (Sørensen, 1997). This mineral assemblage is significantly different from that occurring in miascitic rocks, in which zircon and titanite are characteristic minerals. Typically, eudialyte is found in peralkaline nepheline syenites such as the Khibiny and Lovozero complexes of the Kola Peninsula in Russia, the Ilímaussaq complex of South Greenland, the Tamazeght complex in Morocco, and the Pilanesberg complex in South Africa (Arzamastsev et al., 2005; Mitchell and Liferovich, 2006; Pfaff et al., 2008; Schilling et al., 2009). Rare examples of eudialyte-bearing granites are found at Ascension Island and Straumsvola in Antarctica (Olivo and Williams-Jones, 1999). Eudialyte group minerals may crystallize during the orthomagmatic as well as during late magmatic to hydrothermal stages (Kogarko et al., 1982; Sørensen, 1997; Olivo and Williams-Jones, 1999; Mitchell and Liferovich, 2006; Schilling et al., 2009).

In this work, an analytical technique for the *in situ* determination of Sr, Nd and Hf isotopic ratios in eudialyte group minerals is presented. Our results, which generally compare very well with published solution data, demonstrate that direct *in situ* analysis of eudialyte for U–Pb ages, Sr, Nd and Hf isotopic compositions is generally possible and represents a powerful new method for evaluating the petrogenesis of agpaitic magmatic systems.

2. Analytical methods

Eudialyte from nine localities was analysed for major and trace elements, U and Pb isotopic compositions, and Sr, Nd and Hf isotopic ratios. For an in-house standard, an eudialyte separate was obtained by crushing the rock sample, followed by handpicking the eudialyte crystals. These were embedded in epoxy and polished for subsequent *in situ* analyses. Some clean grains were selected for Sr, Nd and Hf isotopic analyses using isotope dilution (ID) methods in order to check the reliability and feasibility of the *in situ* analyses. All analyses were conducted at the Institute of Geology and Geophysics, Chinese Academy of Sciences.

2.1. Major elements analyses

Major element compositions were obtained using a JEOL-JAX8100 electron microprobe with 15 kV accelerating potential and 12 nA beam current. Counting times were 20 s. Total iron is expressed as FeO. The analytical uncertainties are within 2% for SiO_2, ZrO_2, FeO, CaO and Na_2O, but ~10–20% for other minor elements due to their low concentrations.

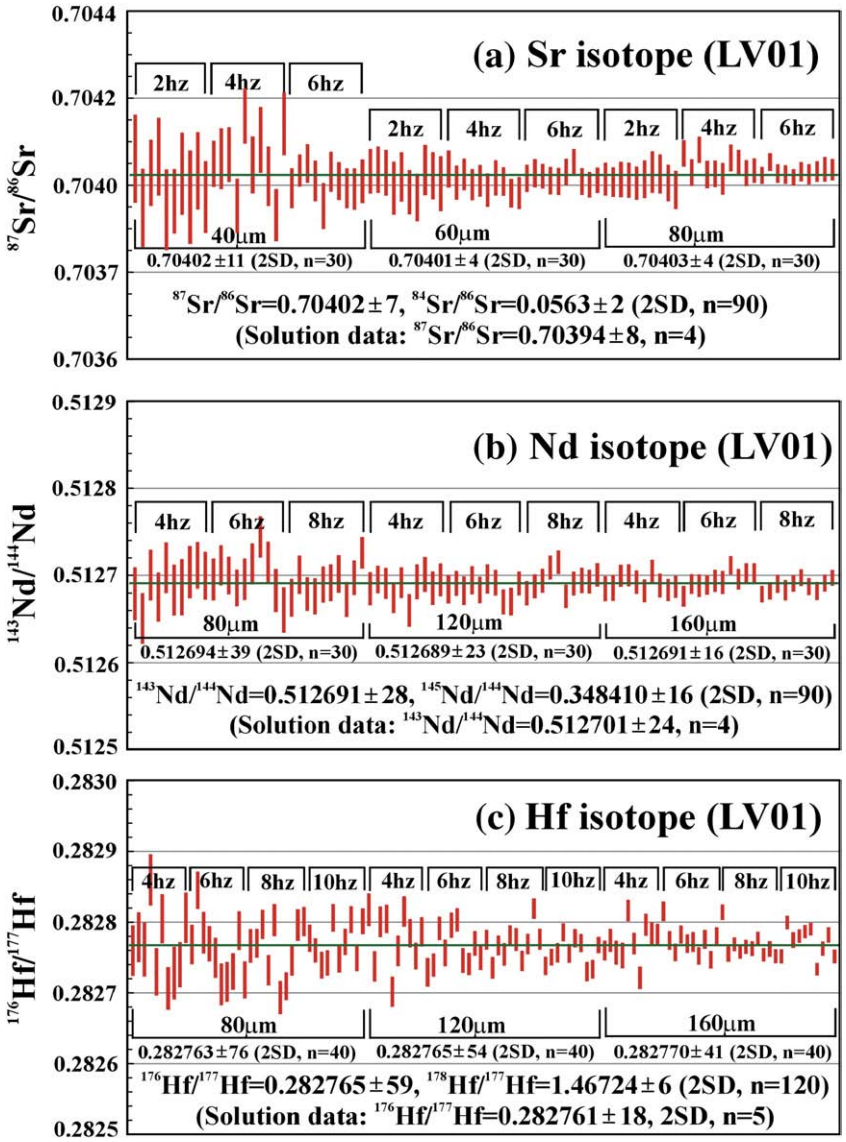

Fig. 1. *In situ* Sr–Nd–Hf isotopic analyses of in-house eudialyte standard of LV01.

Table 1
In situ Sr–Nd–Hf isotopic measurements (2SD) of in-house eudialyte standard (LV01) using different spot sizes and pulse rates.

$^{87}Sr/^{86}Sr$ ratio				
Solution data: $^{87}Rb/^{86}Sr = 0.0016$, $^{87}Sr/^{86}Sr = 0.70394 \pm 8$ (2SD, $n = 4$)				
	40 μm	60 μm	80 μm	Average
2 Hz	0.704000 ± 93	0.704011 ± 46	0.704010 ± 23	0.704007 ± 60
4 Hz	0.704052 ± 146	0.704005 ± 36	0.704041 ± 46	0.704033 ± 97
6 Hz	0.704006 ± 55	0.704018 ± 30	0.704029 ± 20	0.704018 ± 41
Average	0.704020 ± 111	0.704011 ± 38	0.704027 ± 40	**0.704019 ± 72**
$^{143}Nd/^{144}Nd$ ratio				
Solution data: $^{147}Sm/^{144}Nd = 0.1173$, $^{143}Nd/^{144}Nd = 0.512701 \pm 24$ (2SD, $n = 4$)				
	80 μm	120 μm	160 μm	Average
4 Hz	0.512690 ± 37	0.512687 ± 24	0.512691 ± 16	0.512689 ± 26
6 Hz	0.512700 ± 45	0.512685 ± 19	0.512694 ± 19	0.512693 ± 32
8 Hz	0.512691 ± 33	0.512694 ± 24	0.512688 ± 13	0.512691 ± 24
Average	0.512694 ± 39	0.512689 ± 23	0.512691 ± 16	**0.512691 ± 28**
$^{176}Hf/^{177}Hf$ ratio				
Solution data: $^{176}Lu/^{177}Hf = 0.00277$, $^{176}Hf/^{177}Hf = 0.282761 \pm 18$ (2SD, n = 5)				
	80 μm	120 μm	160 μm	Average
4 Hz	0.282766 ± 92	0.282774 ± 75	0.282770 ± 52	0.282770 ± 73
6 Hz	0.282757 ± 85	0.282762 ± 53	0.282772 ± 38	0.282763 ± 61
8 Hz	0.282760 ± 79	0.282768 ± 46	0.282766 ± 37	0.282765 ± 55
10 Hz	0.282769 ± 53	0.282758 ± 37	0.282771 ± 42	0.282765 ± 45
Average	0.282763 ± 76	0.282765 ± 54	0.282770 ± 41	**0.282765 ± 59**

2.2. In situ trace elements and U–Pb analyses

Trace element compositions (including REE) and U–Pb age determinations were conducted using laser ablation inductively coupled plasma mass spectrometry (LA-ICP-MS); the detailed analytical procedures are provided in Xie et al. (2008). The ArF excimer laser ablation system (Geolas CQ) is attached to an Agilent 7500a ICP-MS instrument. With a fluence of ~10 J/cm^2, the selection of spot size (60–160 μm) and repetition rate (3–10 Helz) depended on the signal intensity. During laser ablation, helium gas was flushed into the sample cell to minimize aerosol deposition around the ablation pit and argon gas was then used to improve transport efficiency. The background of ^{204}Pb and ^{202}Hg was less than 100 cps because of the use of high purity liquid argon and helium gas, compared to from <10 to 500 cps for eudialyte depending on its common Pb contents.

ICP-MS measurements were carried out using time-resolved analysis and peak hopping at one point per mass. Every five samples analysed were followed by one standard zircon 91500 and one NIST SRM 610 measurement. Each spot analysis consisted approximately of a 30 s background acquisition and 40 s sample data acquisition. $^{207}Pb/^{206}Pb$, $^{206}Pb/^{238}U$, $^{207}U/^{235}U$ ($^{235}U = ^{238}U/137.88$) and $^{208}Pb/^{232}Th$ ratios were corrected by using zircon 91500 as an external standard. The fractionation correction and results were calculated using GLITTER 4.0 (Griffin et al., 2008). All the measured isotope ratios of zircon 91500 during sample analysis were regressed and corrected using reference values. The relative standard deviations of reference values for zircon 91500 were set at 2%. After obtaining the Pb isotopic ratios, the ^{207}Pb method was applied for common Pb corrections using the upper intercept obtained from a Tera–Wasserburg diagram. Subsequently, $^{206}Pb/^{238}U$ weighted ages were calculated using ISOPLOT 3.0 (Ludwig, 2003). Errors of individual analyses are based on counting statistics and are given at the 1σ level, although errors on pooled ages are quoted at the 2σ or 95% confidence level. Trace element concentrations were calculated using GLITTER 4.0 and calibrated using ^{40}Ca as an internal standard and NIST610 as an external reference material. The analytical uncertainties are mostly within 10%.

2.3. Sr–Nd–Hf analyses by isotope dilution

Chemical separation was undertaken by conventional ion-exchange techniques. The detailed procedure is discussed by Yang et al. (2010), and only a brief introduction is given here. Eudialyte crystals were dissolved with a mixed spike (^{87}Rb–^{84}Sr, ^{149}Sm–^{150}Nd and ^{176}Lu–^{180}Hf) in 2.5 ml concentrated HF, 0.2 ml HNO_3 and $HClO_4$ using

Table 2
Chemical compositions of studied eudialyte, titanite and apatite.

Sample	GM1370	GM1369	KP21	KP58	GM1335	ILM101	KB-0	KB-0 Ap	KB-0 Tit	KB-1	KB-1 Ap	KB-1 Tit	KB-2	KB-3	KB-3 Ap	LV-13
Major elements (wt.%)																
SiO_2	53.64	53.29	54.19	54.94	52.45	52.91	51.50	0.11	32.36	51.29	0.28	31.43	51.31	52.06	0.18	50.61
TiO_2	0.03	0.02	0.01	0.01	0.01	0.01	0.36	0.01	38.16	0.57	0.01	37.60	0.84	0.31	0.01	0.78
ZrO_2	12.63	12.56	12.85	12.97	12.45	12.66	12.64	1.19	0.18	12.98	1.21	0.22	12.45	11.64	1.22	14.39
Nb_2O_5	0.54	0.15	0.54	0.32	0.48	0.35	0.08	0.17	1.24	0.08	0.13	0.35	0.12	0.00	0.03	0.29
La_2O_3	0.41	0.42	0.63	1.01	0.46	0.47	0.03	0.19	0.04	0.03	0.37	0.07	0.04	0.05	0.37	0.24
Ce_2O_3	0.84	0.93	1.51	2.22	0.95	0.87	0.11	0.25	0.09	0.08	0.65	0.24	0.13	0.11	0.62	0.63
Pr_2O_3	0.12	0.09	0.15	0.25	0.14	0.09	0.04	0.05	0.06	0.05	0.09	0.06	0.03	0.05	0.06	0.07
Nd_2O_3	0.33	0.27	0.61	0.94	0.29	0.24	0.00	0.05	0.04	0.00	0.18	0.06	0.00	0.01	0.18	0.02
MgO	0.02	0.02	0.00	0.01	0.02	0.02	0.03	0.01	0.00	0.03	0.01	0.03	0.02	0.07	0.01	0.06
FeO	4.60	4.44	5.13	2.62	6.58	6.46	6.04	0.02	0.72	5.27	0.00	1.12	5.74	6.22	0.02	3.02
MnO	0.84	1.06	1.38	1.77	0.60	0.97	0.74	0.01	0.04	0.35	0.01	0.04	0.55	0.39	0.01	2.77
CaO	10.99	10.81	9.94	8.22	11.11	10.54	12.14	54.41	27.48	11.51	50.21	27.80	11.59	12.12	51.46	7.85
SrO	0.00	0.00	0.00	0.00	0.00	0.00	0.09	2.61	0.03	0.31	7.20	0.13	0.02	0.04	4.51	0.62
Na_2O	12.11	13.53	11.88	12.84	12.22	13.51	14.53	0.10	1.11	14.46	0.18	0.49	14.84	14.10	0.19	17.68
Cl	1.03	1.25	0.46	0.45	1.08	0.94	1.27	0.00	0.00	1.25	0.00	0.01	1.27	0.88	0.00	1.15
Total	98.14	98.84	99.29	98.56	98.82	100.03	99.59	100.80	101.63	98.27	100.31	99.72	98.94	98.04	97.61	100.18
Trace elements (ppm)																
U	67	32	140	253	40	46	44	1.9	4.6	27	1.4	1.7	69	30	1.3	31
Th	35	16	68	79	23	21	18	21	12	15	16	7.8	34	14	20	44
Pb	107	84	1212	80	83	136	24	1.9	1.5	14	1.1	0.76	16	15	1.2	41
Rb	26	9.4	101	31	8.6	37	5.9	0.15	7.8	25	2.0	8.7	4.7	24	0.18	9.8
Sr	147	814	1047	1016	655	649	6575	25895	2138	10579	83976	5403	7642	9132	45663	17928
Sm	913	797	1768	2054	741	772	77	134	98	106	238	172	123	80	259	881
Nd	3770	3676	9262	10901	3560	3602	235	939	467	391	1988	1014	486	287	1937	3218
Lu	181	92	135	128	102	101	22	0.73	0.8	20	0.71	1.0	18	18	0.85	77
Yb	1123	616	957	918	639	638	144	8.1	11	130	8.1	13	131	122	10	498
Hf	2176	2134	1944	1600	2201	2117	1403	0.03	36	1614	0.16	75	1221	1646	0.02	2251

steel-jacketed Teflon bombs placed in an oven for a week at 190 °C. Following complete dissolution and spike-sample homogenization, each sample was dried down at high temperature (fuming $HClO_4$) on a hot plate; then the mixture was treated with 6 M HCl, evaporated to dryness, and taken up in 3 M HCl before chemical separation. The treatment with 6 M HCl is necessary to completely convert fluorides into chlorides (Münker et al., 2001).

The first stage was the separation of Lu and Hf from the matrix using Eichrom Ln-spec resin (100–150 μm, 2 ml), modified from the procedure of Münker et al. (2001). The major element and light and middle rare earth element (L(M)REE) fraction was eluted and collected using 3 M HCl and 4 M HCl for further purification. After collecting the Lu (+Yb) fraction using 4 M HCl, the column was rinsed with 6 M HCl to remove effectively any remaining Lu and Yb before collection of the Hf fraction, followed by separation of Ti from Hf using an $HCl+H_2O_2$ mixture. In addition, the Hf fraction was eluted with 2 M HF. The second stage involved standard cation exchange chromatography for Rb and Sr purification. The L(M)REE eluted with 6 M HCl were further purified using another Eichrom Ln resin (100–150 μm, 2 ml) with 0.25 M HCl for Nd and 0.40 M HCl for Sm, modified from the technique of Pin and Zalduegui (1997). In order to check the reliability of procedure, apatite and titanite from the same rocks were also selected for Sr and Nd isotopic analyses. The chemical separation procedure was similar to that described above except that separation of Lu and Hf was not attempted.

Rb, Sr, Sm and Nd concentrations and Sr–Nd isotopes were analysed using a Finnigan MAT 262 thermal ionization mass spectrometer (TIMS). Procedural blanks were less than 100 pg for Rb and Sr, and 50 pg for Sm and Nd. $^{87}Sr/^{86}Sr$ and $^{143}Nd/^{144}Nd$ ratios were normalized to $^{86}Sr/^{88}Sr=0.1194$ and $^{146}Nd/^{144}Nd=0.7219$ using the exponential law. Isotopic analyses of Lu and Hf were collected using a Neptune MC-ICP-MS and followed the methods of Vervoort et al. (2004). Typical analytical blanks were less than 50 pg for Hf and 10 pg for Lu. Hafnium isotope ratios were corrected for instrumental mass bias to $^{179}Hf/^{177}Hf=0.7325$ using the exponential law. During the period of data acquisition, standard analyses yielded results of $^{87}Sr/^{86}Sr=0.710250\pm11$ (2SD, $n=18$) for NBS987, $^{143}Nd/^{144}Nd=0.512120\pm12$ (2SD, $n=12$) for JNdi-1, and $^{176}Hf/^{177}Hf=0.282165\pm10$ (2SD, $n=10$) for JMC475. In addition, USGS reference materials BCR-1 and BHVO-2 were also processed for Sr–Nd–Hf isotopes, and gave ratios of 0.704977 ± 12 and 0.703474 ± 11 for $^{87}Sr/^{86}Sr$, 0.512655 ± 5 and 0.513000 ± 15 for $^{143}Nd/^{144}Nd$ and 0.282866 ± 6 and 0.283109 ± 5 for $^{176}Hf/^{177}Hf$, respectively, which is identical, within error, to the recommended values (Weis et al., 2005, 2006, 2007).

2.4. In situ Sr–Nd–Hf isotopic analyses by laser ablation

The *in situ* Sr–Nd–Hf isotopic analyses were conducted using the Neptune MC-ICP-MS machine. Detailed analytical protocols were given by Yang et al. (2007, 2009) and Wu et al. (2006), only a brief review is given here.

The *in situ* Sr isotopic data were acquired in static, multi-collector mode with low resolution using nine Faraday collectors, and the mass configuration array from ^{83}Kr to ^{88}Sr. During analyses, a 50 s measurement of the gas blank was carried out prior to ablation in order to correct for Kr assuming $^{83}Kr/^{84}Kr=0.20175$ and $^{83}Kr/^{86}Kr=0.66474$. The natural ratio of $^{85}Rb/^{87}Rb$ of 2.5926 was used for isobaric correction of Rb by the exponential law, assuming that rubidium has the same mass discrimination as strontium (Ehrlich et al., 2001). No correction was applied for the interference of Ca argide/dimer species as our experiments demonstrated that this interference is negligible (e. g., Ehrlich et al., 2001; Fortunato et al., 2004; Ramos et al., 2004; Vroon et al., 2008). Interferences from Fe dioxides, and Ga and Zn oxides, are not considered in this study, due to their low signals during actual analyses. However, interference from the doubly charged rare earth elements (REEs) is not negligible when eudialyte was ablated for Sr and Nd isotopic measurements, due to the high concentrations of REEs. Based on the method proposed by Ramos et al. (2004), we monitored the presence of $^{167}Er^{2+}$, $^{171}Yb^{2+}$ and $^{173}Yb^{2+}$ at masses 83.5, 85.5 and 86.5. Then the contributions of $^{168}Er^{2+}$ and $^{168}Yb^{2+}$ to ^{84}Sr, $^{170}Er^{2+}$ and $^{170}Yb^{2+}$ to ^{85}Sr ($+^{85}Rb$), $^{172}Yb^{2+}$ to ^{86}Sr, $^{174}Yb^{2+}$ to ^{87}Sr

LV01	LV02	LV03	LV04	SM6	SM06 Tit	SM7	SM25	TMZ177	TMZ241	TMZ298	MSH38	MSH52	PDC	KPW	LGS	LGS Ap
54.41	52.62	53.14	52.87	52.96	31.93	53.76	57.38	54.56	51.94	51.82	49.33	48.80	55.00	52.91	50.30	0.45
0.55	0.44	0.45	0.44	0.28	37.80	0.31	0.24	0.28	0.22	0.30	0.13	0.01	0.54	0.30	0.09	0.00
12.47	12.34	12.42	11.95	11.92	0.26	11.94	13.22	13.59	12.19	12.17	11.58	11.71	12.02	11.79	11.82	1.22
0.08	0.17	0.03	0.05	0.13	0.28	0.17	0.25	0.67	0.18	0.64	1.48	2.09	0.57	0.21	1.22	0.10
0.39	0.33	0.31	0.30	0.20	0.14	0.12	0.56	0.49	0.32	0.10	1.04	0.88	0.22	0.28	0.80	0.52
0.71	0.71	0.70	0.68	0.35	0.53	0.27	1.20	0.51	0.36	0.12	1.85	1.41	0.26	0.54	0.93	1.14
0.07	0.11	0.04	0.13	0.06	0.07	0.08	0.15	0.08	0.03	0.04	0.16	0.11	0.06	0.08	0.09	0.11
0.09	0.14	0.11	0.13	0.06	0.22	0.03	0.26	0.00	0.00	0.00	0.08	0.05	0.00	0.15	0.03	0.40
0.06	0.09	0.06	0.08	0.07	0.01	0.06	0.04	0.01	0.03	0.02	0.05	0.01	0.05	0.08	0.04	0.01
3.24	4.93	4.77	5.00	6.57	0.99	6.88	4.08	4.16	5.14	5.62	4.58	6.22	3.39	2.35	6.25	0.02
2.56	2.06	2.14	1.97	1.02	0.04	0.85	2.28	4.07	2.75	1.86	4.88	3.05	3.81	1.31	2.65	0.03
10.41	10.08	10.18	10.15	10.90	26.56	11.09	7.85	10.38	10.53	13.40	8.82	10.27	11.03	12.77	11.83	56.01
0.41	0.09	0.17	0.31	1.79	0.51	1.91	1.60	0.29	0.78	1.66	0.28	0.00	1.59	0.00	0.00	0.14
14.30	15.13	14.59	15.17	12.64	0.86	12.85	8.06	10.20	14.09	11.57	13.14	14.01	10.89	12.79	11.71	0.27
0.71	0.74	0.75	0.69	0.95	0.01	0.86	0.62	0.18	0.65	0.64	0.42	1.00	0.88	0.55	0.67	0.01
100.45	99.97	99.86	99.92	99.89	100.29	101.19	97.80	99.46	99.21	99.96	97.82	99.63	100.30	96.11	98.42	101.40
66	34	38	41	77	39	388	475	346	69	41	82	42	40	53	23	18
66	23	24	23	64	46	650	264	173	35	19	129	36	26	26	204	161
30	35	32	31	146	13	105	68	242	163	95	207	109	40	112	472	10
7.8	7.8	8.8	8.7	6.4	1.0	6.9	12	28	17	16	13	15	34	45	15	0.31
13606	10289	11491	10731	27323	9219	25352	22514	15250	14132	25699	10796	108	21913	1405	2409	1518
678	503	532	523	292	360	279	874	78	58	19	714	530	45	858	188	547
3887	2815	3068	2879	1261	2101	1081	4260	843	482	169	4918	3253	331	2526	1479	4107
58	44	43	43	44	0.54	52	38	13	28	11	60	130	14	577	71	6.8
392	293	292	288	257	7.4	302	248	77	151	63	423	750	78	4577	445	59
2986	2321	2451	2432	2510	134	2314	2235	1165	1149	1355	1561	1903	1924	2029	4226	0.17

($+^{87}Rb$), and $^{176}Yb^{2+}$ to ^{88}Sr were calculated according to the isotopic abundances of Er and Yb (Chartier et al., 1999; Vervoort et al., 2004). However, no corrections of $^{176}Lu^{2+}$ and $^{176}Hf^{2+}$ on ^{88}Sr were made in this study since their signal intensities are low. During our data reduction, the effects of interfering elements were accounted for in the order of Kr, Yb^{2+}, Er^{2+} and Rb. In order to avoid the potential matrix-matched effect during laser ablation, an in-house eudialyte standard (LV01) was used for external correction during analyses.

The laser ablation Nd isotope technique is similar to that for Sr isotope analysis described above. Before analysis, a standard Nd solution was used to calibrate the machine using the exponential law for mass bias correction and assuming $^{146}Nd/^{144}Nd = 0.7219$. For *in situ* Nd isotopic analyses, the interferences are principally caused by Ce (^{142}Ce on ^{142}Nd) and Sm (^{144}Sm on ^{144}Nd). Our previous work indicated that the influence of Ce on Nd isotope analysis is insignificant when the Ce/Nd ratio is ≤3, which is the normal value in natural geological materials (Yang et al., 2007). For the interference of ^{144}Sm on ^{144}Nd, the mass bias of Sm (β_{Sm}) was directly obtained from the $^{147}Sm/^{149}Sm$ ratio on the sample itself and then applied in the isobaric interference correction, following the method proposed by McFarlane and McCulloch (2007), but with constant values of $^{147}Sm/^{149}Sm = 1.08680$ and $^{144}Sm/^{149}Sm = 0.22332$ (Yang et al., 2008). In addition, the stable $^{145}Nd/^{144}Nd$ ratio of 0.348415 was used to evaluate the feasibility of our method. In order to evaluate measurement and potential matrix-matched effects, in-house standard of eudialyte (LV01) was used for external correction.

During Hf isotopic analyses, the isobaric interference of ^{176}Lu on ^{176}Hf is minor due to the low $^{176}Lu/^{177}Hf$ in eudialyte (normally <0.01, which corresponds to a Lu/Hf ratio of ~0.07). In this study, $^{176}Lu/^{175}Lu = 0.02655$ was used to extract the interference of ^{176}Lu to ^{176}Hf. However, the interference of ^{176}Yb on ^{176}Hf must be carefully corrected since the contribution of ^{176}Yb to ^{176}Hf could profoundly affect the accuracy of the measured $^{176}Hf/^{177}Hf$ ratio. We used the mean $^{173}Yb/^{172}Yb$ ratio of the individual spots to calculate the fractionation coefficient (β_{Yb}) and the contribution of ^{176}Yb to ^{176}Hf (Wu et al., 2006) by applying ratios of $^{176}Yb/^{172}Yb = 0.5887$ and $^{173}Yb/^{172}Yb = 0.73925$. Zircon standard of 91500 and an in-house eudialyte standard of LV01 were used for external correction. During analytical sessions, the obtained $^{176}Hf/^{177}Hf$ value for 91500 was 0.282301 ± 3 (2σ, $n = 114$) or 0.282303 ± 28 (2SD), which is similar to the values obtained by the solution method within error (Wiedenbeck et al., 1995; Woodhead et al., 2004; Wu et al., 2006; Blichert-Toft, 2008). For the in-house eudialyte standard, the details are described below.

3. Sr–Nd–Hf isotopic analyses of the in-house standard

Currently, there is no eudialyte isotopic standard. To check the reliability of our methods, an in-house eudialyte standard (termed LV01) was analysed by solution and laser ablation methods. This standard eudialyte, with a grain-size of $\sim 10 \times 8 \times 6\ mm^3$, originates from a pegmatitic syenite occurring in the Lovozero alkaline complex (Kola, Russia).

The Sr isotopic analysis was carried out with spot sizes of 40, 60 and 80 μm and repetition pulse rates of 2, 4 and 6 Hz. Each ten measurements were collected and the average $^{87}Sr/^{86}Sr$ ratios, with 2SD are reported (Fig. 1a, Table 1). As can be seen in Table 1, signal intensity increases with spot size, resulting in a higher precision for a larger spot size. There is no correlation between the pulse rate and data precision (Fig. 1a) and the obtained $^{87}Sr/^{86}Sr$ ratios for three different spot sizes are identical within error, with an average value of 0.70402 ± 7 (2SD, $n = 90$) (Fig. 1a). The average $^{84}Sr/^{86}Sr$ ratio of 0.0563 ± 2 (2SD, $n = 90$) is identical to the theoretical value of 0.0565 within error. Using the solution method, LV01 has an $^{87}Sr/^{86}Sr$ ratio of

Table 3
In situ laser ablation Sr–Nd–Hf isotopic data of eudialyte, titanite and apatite.

Sample	Location	Mineral	U–Pb age	$^{87}Rb/^{86}Sr$	$^{87}Sr/^{86}Sr$	2σ	I_{Sr}	$^{147}Sm/^{144}Nd$	$^{143}Nd/^{144}Nd$	2σ	$\varepsilon_{Nd}(t)$	2σ	$^{176}Lu/^{177}Hf$	$^{176}Hf/^{177}Hf$	2σ	$\varepsilon_{Hf}(t)$	2σ
GM1370	Ilimaussaq	Eudialyte	1041 ± 17					0.1462	0.512193	12	−1.18	0.23	0.00842	0.282337	15	3.81	0.53
GM1369	Ilimaussaq	Eudialyte	1108 ± 21	0.01860	0.70853	3	0.7082	0.1346	0.512083	10	−1.61	0.20	0.00467	0.282232	9	3.00	0.32
KP21	Ilimaussaq	Eudialyte	1018 ± 34					0.1396	0.512067	21	−2.66	0.41					
KP58	Ilimaussaq	Eudialyte	1102 ± 12					0.1327	0.512049	9	−1.99	0.18					
GM1335	Ilimaussaq	Eudialyte	1118 ± 28					0.1288	0.512044	12	−1.50	0.23	0.00496	0.282239	9	3.02	0.32
ILM101	Ilimaussaq	Eudialyte	1134 ± 29					0.1325	0.512059	11	−1.76	0.21	0.00512	0.282250	13	3.29	0.46
KB-0	Khibiny	Eudialyte	368 ± 7	0.00261	0.70350	2	0.7035	0.2044	0.512933	6	5.40	0.12	0.00164	0.282804	10	8.88	0.35
KB-0 (Tit)	Khibiny	Titanite	369 ± 10	0.00015	0.70339	2	0.7034	0.1362	0.512720	13	4.46	0.25					
KB-0 (Ap)	Khibiny	Apatite	361 ± 15	0.00001	0.70343	2	0.7034	0.0932	0.512611	18	4.37	0.35					
KB-1	Khibiny	Eudialyte	365 ± 8	0.00764	0.70346	1	0.7035	0.1653	0.512853	11	5.68	0.21	0.00140	0.282797	9	8.69	0.32
KB-1 (Tit)	Khibiny	Titanite	351 ± 17	0.00007	0.70318	2	0.7032	0.1101	0.512689	7	5.09	0.14					
KB-1 (Ap)	Khibiny	Apatite	357 ± 16	0.00004	0.70327	2	0.7033	0.0775	0.512579	9	4.49	0.18					
KB-2	Khibiny	Eudialyte	358 ± 9	0.00156	0.70339	1	0.7034	0.1648	0.512826	6	5.18	0.12	0.00203	0.282805	7	8.82	0.25
KB-3	Khibiny	Eudialyte	362 ± 9	0.00368	0.70343	2	0.7034	0.1861	0.512868	10	4.99	0.20	0.00149	0.282806	9	8.98	0.32
KB-3 (Ap)	Khibiny	Apatite	355 ± 21	0.00001	0.70325	2	0.7032	0.0852	0.512592	9	4.38	0.18					
KB-3 (Ap)	Khibiny	Apatite						0.0860	0.512609	4	4.67	0.08					
LV13	Lovozero	Eudialyte	371 ± 29	0.00208	0.70378	1	0.7038	0.1641	0.512739	6	3.51	0.12	0.00363	0.282741	9	6.16	0.32
LV01	Lovozero	Eudialyte	376 ± 6	0.00247	0.70395	1	0.7039	0.1240	0.512672	5	4.10	0.10	0.00254	0.282788	12	8.09	0.42
LV02	Lovozero	Eudialyte	359 ± 8	0.00353	0.70400	2	0.7040	0.1221	0.512662	8	4.00	0.16	0.00260	0.282775	10	7.61	0.35
LV03	Lovozero	Eudialyte	361 ± 15	0.00306	0.70404	1	0.7040	0.1212	0.512665	7	4.10	0.14	0.00267	0.282789	5	8.09	0.18
LV04	Lovozero	Eudialyte	373 ± 7	0.00286	0.70403	2	0.7040	0.1239	0.512666	7	3.99	0.14	0.00262	0.282790	13	8.14	0.46
SM06	Saima	Eudialyte	209 ± 14	0.00079	0.70855	2	0.7086	0.1422	0.511929	8	−12.27	0.16	0.00203	0.282318	8	−11.42	0.28
SM06(Tit)	Saima	Titanite	224 ± 5	0.00005	0.70833	3	0.7083	0.1211	0.511872	13	−12.78	0.25					
SM07	Saima	Eudialyte	224 ± 4	0.00085	0.70854	1	0.7085	0.1537	0.511928	6	−12.62	0.12	0.00149	0.282335	13	−10.74	0.46
SM25	Saima	Eudialyte	193 ± 3	0.00158	0.70857	2	0.7086	0.1329	0.511896	10	−12.65	0.20	0.00198	0.282348	10	−10.35	0.35
TMZ 177	Tamazeght	Eudialyte	40 ± 5	0.00668	0.70324	2	0.7032	0.0588	0.512814	7	4.21	0.14	0.00143	0.282912	9	5.87	0.32
TMZ 241	Tamazeght	Eudialyte	43 ± 35	0.00420	0.70336	2	0.7034	0.0742	0.512807	7	3.98	0.14	0.00251	0.282875	6	4.53	0.21
TMZ 298	Tamazeght	Eudialyte	43 ± 24	0.00236	0.70320	2	0.7032	0.0741	0.512837	14	4.57	0.27	0.00110	0.282905	8	5.64	0.28
MSH 38	Mt-St Hilaire	Eudialyte	128 ± 12	0.00580	0.70385	3	0.7038	0.1107	0.512789	8	4.37	0.16	0.00548	0.283033	14	11.62	0.50
MSH 52	Mt-St Hilaire	Eudialyte	137 ± 17					0.0980	0.512811	6	5.01	0.12	0.00788	0.282949	14	8.44	0.50
PDC	Poços de Caldas	Eudialyte	77 ± 13	0.00457	0.70529	2	0.7053	0.0851	0.512413	10	−3.25	0.20	0.00077	0.282653	11	−2.49	0.39
KPW	Kipawa	Eudialyte	1012 ± 16					0.2438	0.512403	6	−10.64	0.12					
LGS	Langesundsfjord	Eudialyte						0.0847	0.512610	6	3.17	0.12	0.00246	0.282833	7	7.45	0.25
LGS	Langesundsfjord	Apatite	260 ± 4	0.00029	0.70366	2	0.7037	0.0913	0.512667	18	4.07	0.35					

Table 4
Solution Sr–Nd–Hf isotopic data of eudialyte, titanite and apatite.

Sample	Mineral	Rb	Sr	$^{87}Rb/^{86}Sr$	$^{87}Sr/^{86}Sr$	2σ	I_{Sr}	Sm	Nd	$^{147}Sm/^{144}Nd$	$^{143}Nd/^{144}Nd$	2σ	$\varepsilon_{Nd}(t)$	2σ	Lu	Hf	$^{176}Lu/^{177}Hf$	$^{176}Hf/^{177}Hf$	2σ	$\varepsilon_{Hf}(t)$	2σ
GM1370	Eud	54	134	1.1607	0.732185	26	0.7129	737	3012	0.1478	0.512164	7	−1.99	0.13	84.8	1352	0.0089	0.282318	5	2.75	0.18
GM1370	Eud-R	57	143	1.1675	0.730879	31	0.7115	748	3216	0.1407	0.512145	6	−1.30	0.12							
KP21	Eud	134	852	0.4557	0.728132	36	0.7206	1380	6521	0.1279	0.512087	7	−0.53	0.15	91.8	1305	0.0100	0.282416	6	5.38	0.20
KP58	Eud							1880	8981	0.1266	0.512070	13	−0.66	0.25	89.0	961	0.0132	0.282360	4	0.97	0.13
KB-0	Eud-1	6.5	6680	0.0028	0.703511	16	0.7035	71	222	0.1930	0.512949	7	6.25	0.14	16.1	1150	0.0020	0.282815	4	9.16	0.14
KB-0	Eud-1R1														19.3	1138	0.0024	0.282809	4	8.86	0.14
KB-0	Eud-1R2														18.6	1140	0.0023	0.282811	4	8.97	0.14
KB-0	Eud-2	6.4	6498	0.0028	0.703430	12	0.7034	69	218	0.1919	0.512896	16	5.27	0.31	13.2	931	0.0020	0.282813	6	9.09	0.21
KB-0	Eud-2R1														18.4	917	0.0028	0.282808	7	8.70	0.25
KB-0	Eud-2R2														17.0	922	0.0026	0.282797	7	8.39	0.25
KB-0	Eud-3	6.5	6477	0.0029	0.703460	16	0.7034	69	217	0.1914	0.512933	6	6.01	0.11	15.2	963	0.0022	0.282811	5	8.97	0.18
KB-0	Eud-3R														16.5	955	0.0025	0.282809	4	8.86	0.13
KB-0	Tit	1.17	2307	0.0015	0.703373	9	0.7034	99	479	0.1251	0.512712	11	4.84	0.21							
KB-0	Ap	0.46	38128	0.0000	0.703415	13	0.7034	118	847	0.0845	0.512648	10	5.51	0.20							
KB-1	Eude	32.7	11225	0.0084	0.703548	12	0.7035	100	374	0.1618	0.512863	6	6.04	0.11	14.2	854	0.0024	0.282814	4	9.05	0.14
KB-1	Eud-R														14.2	856	0.0024	0.282820	5	9.26	0.18
KB-1	Tit	5.47	5042	0.0031	0.703288	15	0.7033	153	877	0.1052	0.512691	12	5.37	0.24							
KB-1	Ap	4.01	115630	0.0001	0.703324	11	0.7033	305	2495	0.0738	0.512644	7	5.93	0.14							
KB-3	Eud-1	12.0	8724	0.0040	0.703412	29	0.7034	80	284	0.1702	0.512874	10	5.86	0.19	14.2	1243	0.0016	0.282811	6	9.14	0.21
KB-3	Eud-1R														15.0	1252	0.0017	0.282812	6	9.15	0.20
KB-3	Eud-2	11.9	8832	0.0039	0.703397	16	0.7034	80	285	0.1699	0.512919	15	6.76	0.29	13.4	1270	0.0015	0.282808	7	9.05	0.25
KB-3	Eud-2R														16.9	1272	0.0019	0.282810	6	9.03	0.21
KB-3	Ap-1	0.55			0.703357	20		253	1913	0.0799	0.512632	10	5.41	0.20							
KB-3	Ap-2	13.4	51806	0.0008	0.703301	23	0.7033	229	1704	0.0812	0.512628	12	5.27	0.24							
KB-3	Ap-3	49.9	70067	0.0021	0.703316	12	0.7033	204	1551	0.0794	0.512641	8	5.61	0.17							
LV13	Eud	16.1	17682	0.0026	0.703690	15	0.7037	724	2752	0.1591	0.512775	8	4.45	0.16	45.7	1317	0.0049	0.282741	4	5.83	0.14
LV01	Eud-1	6.56	11480	0.0017	0.703911	11	0.7039	492	2541	0.1170	0.512706	11	5.10	0.21	31.7	1674	0.0027	0.282764	5	7.22	0.18
LV01	Eud-1R				0.703926	16					0.512714	10			31.7	1674	0.0027	0.282768	5	7.33	0.18
LV01	Eud-1R														31.7	1682	0.0027	0.282770	4	7.40	0.14
LV01	Eud-2	6.38	12088	0.0015	0.703930	15	0.7039	489	2499	0.1184	0.512687	11	4.66	0.21	32.4	1620	0.0028	0.282751	4	6.70	0.13
LV01	Eud-2R														32.4	1629	0.0028	0.282752	5	6.75	0.18
SM06	Eud	6.90	28133	0.0007	0.708506	13	0.7085	251	1098	0.1384	0.511928	9	−12.18	0.18	28.5	1500	0.0027	0.282334	3	−10.96	0.12
SM06	Eud-R														28.5	1505	0.0027	0.282335	4	−10.92	0.14
SM06	Tit	1.9	5062	0.0011	0.708338	11	0.7083	178	1054	0.1020	0.511876	10	−12.15	0.19							
TMZ177	Eud	21.1	13623	0.0045	0.703252	17	0.7032	47	504	0.0569	0.512836	10	4.65	0.19	7.92	841	0.0013	0.282933	9	6.62	0.32
TMZ177	Eud-R														7.92	841	0.0013	0.282936	7	6.74	0.25
MSH52	Eud	24.1	731	0.0954	0.704307	14	0.7041	543	3620	0.0908	0.512804	8	4.99	0.16	83.4	1748	0.0068	0.283059	11	12.41	0.41
MSH52	Eud														83.4	1737	0.0068	0.283056	11	12.33	0.39
MSH52	Eud														83.4	1742	0.0068	0.283054	7	12.23	0.25
KPW	Eud	37	1237	0.087	0.740378	24	0.7391	756	2198	0.2079	0.512205	6	−9.90	0.12	257	960	0.0380	0.282692	3	−6.06	0.11
LGS	Eud	13.8	1776	0.0224	0.703934	13	0.7039	223	1519	0.0888	0.512648	13	3.77	0.26	49.8	1912	0.0037	0.282828	3	7.07	0.11
LGS	Eud-R1														49.8	2046	0.0035	0.282841	3	7.58	0.11
LGS	Eud-R2														49.8	1960	0.0036	0.282837	4	7.39	0.14

0.70394 ± 8 (2SD, $n = 4$) (Fig. 1), identical to that obtained by laser ablation within errors.

For Nd isotopes, larger spot sizes of 80, 120 and 160 μm and repetition pulse rates of 4, 6 and 8 Hz were used. These data yield a weighted average $^{143}Nd/^{144}Nd$ ratio of 0.512691 ± 28 (2SD, $n = 90$) (Fig. 1b, Table 1). The obtained average $^{145}Nd/^{144}Nd$ ratio of 0.348410 ± 16 (2SD, $n = 90$) is identical to the theoretical value of 0.348415 within error. In common with the Sr isotopic analyses, there are no significant variations for the $^{143}Nd/^{144}Nd$ ratios obtained under different spot sizes with different pulse rates. Using the solution method, LV01 has a $^{143}Nd/^{144}Nd$ ratio of 0.512701 ± 24 (2SD, $n = 4$) with $^{147}Sm/^{144}Nd$ of 0.1173 (Fig. 1), consistent with the laser ablation data.

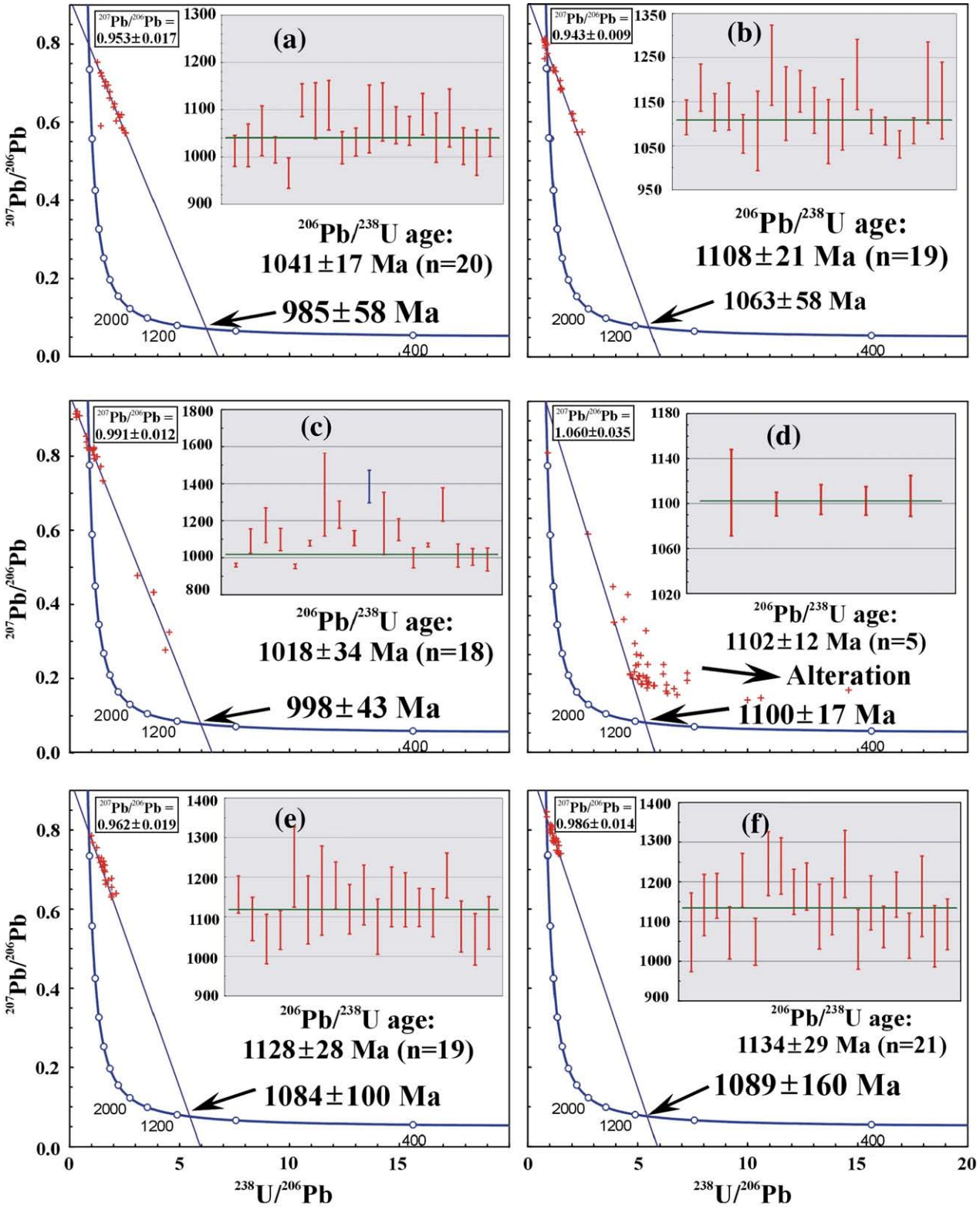

Fig. 2. U–Pb ages and common Pb isotopic composition of eudialyte from the Ilímaussaq complex, Greenland. (a) GM1370; (b) GM1369; (c) KP21; (d) KP58; (e) GM1335 and (f) ILM101.

For Hf isotopes, spot sizes of 80, 120 and 160 μm and repetition pulse rates of 4, 6, 8 and 10 Hz were used. All analyses yield a weighted average $^{176}Hf/^{177}Hf$ ratio of 0.282765 ± 59 (2SD, $n = 120$), which is identical to the solution value of 0.282761 ± 18 (2SD, $n = 5$, Fig. 1c, Table 1). $^{176}Hf/^{177}Hf$ ratios obtained with large spot sizes and high pulse rates are more precise than those obtained with smaller spot sizes and low repetition rates. The average $^{178}Hf/^{177}Hf$ ratio is 1.467246 (2SD, $n = 120$), identical to the theoretical value of 1.8867 within error.

In summary, laser ablation of LV01 gives identical Sr, Nd and Hf isotopic ratios compared to those obtained by solution technique within analytical errors (Fig. 1, Table 1), indicating that our analytical protocol is reliable. Thus, eudialyte LV01 was used for external correction during *in situ* laser ablation analysis for Sr, Nd and Hf isotopic compositions.

4. Applications

In this study, eudialytes from nine agpaitic complexes were investigated. The descriptions of samples and their host complexes are given in the Appendix A. Representative major and trace element compositions of the eudialytes from the different samples are given in Table 2. As the focus of this work is determination of the isotopic composition of eudialyte we have not followed the detailed major element nomenclature of eudialyte group minerals as proposed by Johnsen et al. (2003), and refer to the material investigated simply as eudialyte (sensu lato). The *in situ* Sr, Nd and Hf isotopic data for the analysed eudialytes, together with apatites and titanites from the same samples, are summarized in Table 3. In order to check the reliability of our data, some minerals (eudialyte, apatite and titanite) were selected for solution analysis; these data are given in Table 4.

4.1. Ilímaussaq syenite, Greenland

In the Tera–Wasserburg concordia diagrams (Fig. 2), eudialytes from Ilímaussaq have high common Pb contents. With the exception of KP58, the lower intercept ages range from 985 ± 58 (GM1370) to 1089 ± 160 (ILM101) Ma. Using the common Pb composition determined by the upper intercept, the ^{207}Pb corrected $^{206}Pb/^{238}U$ weighted ages vary from 1018 ± 34 (KP21) to 1134 ± 29 (ILM101) Ma (Fig. 2). Eudialyte from sample KP58 shows a significant deviation from the ~1100 Ma discordia line, indicating Pb loss due to later alteration. However, five analyses of the least altered areas define a line with a lower intercept age of 1100 ± 17 Ma, and ^{207}Pb corrected $^{206}Pb/^{238}U$ weighted age of 1102 ± 12 Ma (Fig. 2d). Considering that ILM101 is a late aplite dyke, it is concluded that the Ilímaussaq complex was emplaced before ~1134 Ma. The above ages were calculated from $^{206}Pb/^{238}U$ ratios. For Precambrian minerals, the $^{207}Pb/^{206}Pb$ age is usually used as later Pb loss would result in "younging" of the $^{206}Pb/^{238}U$ age, but not the $^{207}Pb/^{206}Pb$ age. However, the high common Pb content makes it impossible to calculate the $^{207}Pb/^{206}Pb$ age in this study as a ^{207}Pb correction was used. Therefore, the present data support the conclusion that the emplacement of Ilímaussaq complex took place at ~1160 Ma, as constrained by the baddeleyite and zircon U–Pb ages of the earlier augite syenite and alkali granite, respectively (Upton et al., 2003; Krumrei et al., 2006).

Most of the samples have relatively high Rb/Sr ratios of 0.012 to 0.174 (Table 2), hence it is not possible to determine Sr isotopic compositions by *in situ* analysis as samples with Rb/Sr > 0.02 cannot be accurately corrected for the Rb interference (Yang et al., 2009). Using 160 μm size of laser spot, the $^{87}Sr/^{86}Sr$ isotopic ratio for eudialyte in GM1369 is 0.7085 ± 3 with an $^{87}Rb/^{86}Sr$ ratio of 0.019 ± 1 ($n = 8$, Fig. 3a), confirming the previous conclusion that the Ilímaussaq complex has a high initial Sr isotopic composition of ~0.71 (Blaxland et al., 1976; Waight et al., 2002).

The Nd isotopic analyses show significant variations in $^{147}Sm/^{144}Nd$ and $^{143}Nd/^{144}Nd$ ratios, located along the reference line of 1160 Ma (Fig. 3b). The $\varepsilon_{Nd}(t)$ values range from −2.7 ± 0.4 to −1.2 ± 0.2, and are very similar to the published $\varepsilon_{Nd}(t)$ values of −3.6 ± 0.5 to +0.8 ± 0.5 obtained from whole-rock and mineral analyses (Blaxland et al., 1976; Paslick et al., 1993; Stevenson et al., 1997; Marks et al., 2004). Eudialytes from three samples (GM1370, KP21 and KP58) were also analysed by solution methods and gave similar $\varepsilon_{Nd}(t)$ values (between −2.0 ± 0.1 to −0.5 ± 0.2) compared to those obtained by laser ablation.

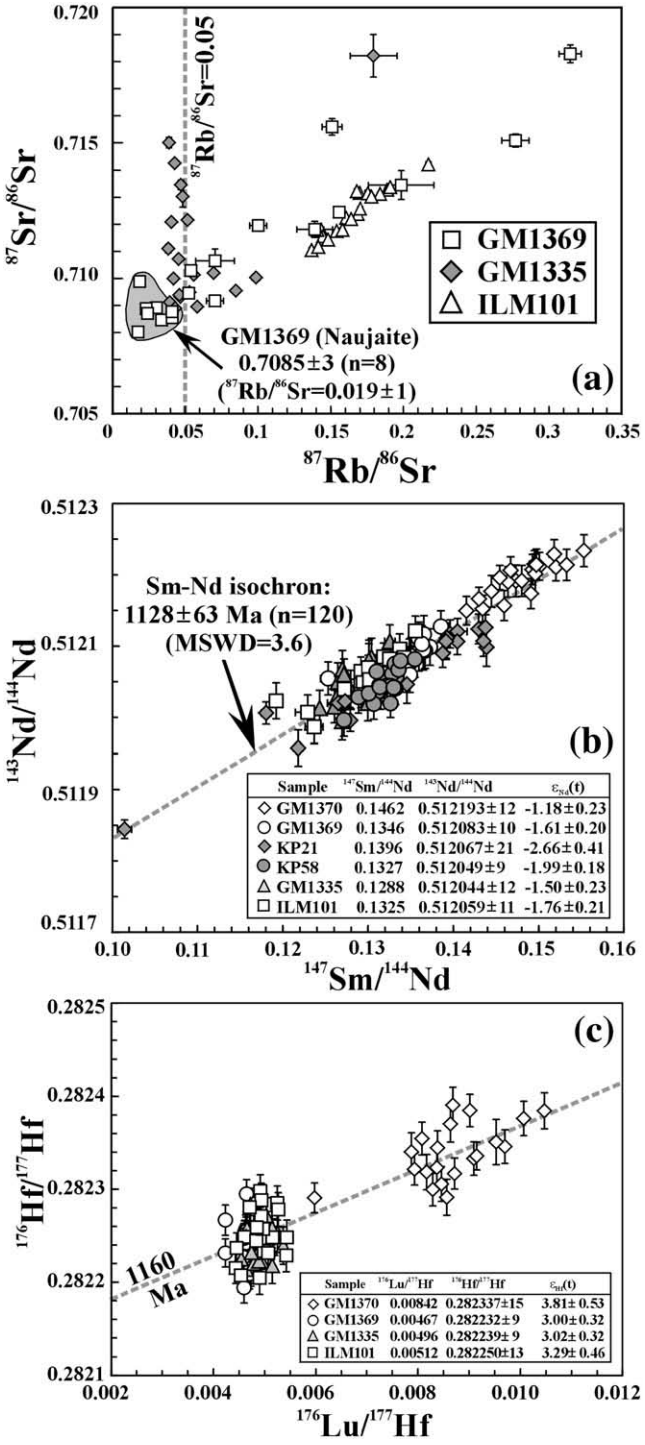

Fig. 3. Sr–Nd–Hf isotopic composition of eudialyte from the Ilímaussaq complex, Greenland. (a) Sr isotopic data; (b) Nd isotopic data; and (c) Hf isotopic data.

Principally, the high Hf concentrations of 1600–2201 ppm should make it possible to obtain precise Hf isotopic ratios for these samples. However, samples KP21 and KP58 have high Yb concentrations making it impossible to correct for the interferences of ^{176}Yb on ^{176}Hf during *in situ* laser ablation analysis (see above). The other samples

have $\varepsilon_{Hf}(t)$ values ranging from $+3.0\pm0.5$ to $+3.8\pm0.5$ (Fig. 3c), identical to the value of $+4.3\pm0.7$ obtained by Patchett et al. (1981). Similarly, the $\varepsilon_{Hf}(t)$ values obtained from the solution data ($+5.4\pm1.0$) are comparable to those by laser ablation.

4.2. Khibiny syenite, Kola Peninsula, Russia

Eudialytes from Khibiny have higher Sr (6575–10579 ppm), and lower Rb (4.7–25 ppm), Sm (77–123 ppm), Nd (235–486 ppm) and Lu (18–22 ppm) concentrations than those from the Ilímaussaq complex. In the Tera–Wasserburg U–Pb diagram (Fig. 4), the lower intercept ages for eudialytes are from 354 ± 27 to 365 ± 23 Ma, with ^{207}Pb corrected ^{206}Pb/^{238}U ages from 356 ± 11 to 365 ± 10 Ma. For sample KB-0, however, if data for titanite and apatite are combined with the eudialyte data, the lower intercept and ^{207}Pb corrected ^{206}Pb/^{238}U ages are 368 ± 11 and 368 ± 5 Ma (Fig. 4a). Similarly, for sample KB-1, the combined analyses of eudialyte, titanite and apatite yield a lower intercept age of 363 ± 15 Ma, and a ^{207}Pb corrected ^{206}Pb/^{238}U age of 361 ± 6 Ma (Fig. 4b). Additionally, analyses of eudialyte and apatite with one exception from sample KB-3 yield lower intercept and ^{207}Pb corrected ^{206}Pb/^{238}U ages of 369 ± 20 and 365 ± 8 Ma (Fig. 4d). These age data are consistent with those previously obtained by zircon U–Pb, whole-rock Rb–Sr and mineral Ar–Ar methods (Kramm et al., 1993; Kramm and Kogarko, 1994; Arzamastsev et al., 2007).

In contrast to the Ilímaussaq complex, eudialytes from Khibiny have much high Sr contents (6575–10579 ppm) with low Rb/Sr ratios (0.0006 to 0.0023) and the ^{87}Sr/^{86}Sr ratios varying from 0.70339 ± 1 to 0.70350 ± 2. Titanite and apatite have slightly lower ^{87}Rb/^{86}Rb and ^{87}Sr/^{86}Sr ratios than those of eudialyte from the same samples; an observation verified by solution analyses (Fig. 5a, Table 4).

Eudialytes from Khibiny show significant variations of ^{147}Sm/^{144}Nd and ^{143}Nd/^{144}Nd ratios located along the reference line of 370 Ma (Fig. 5b), the age of emplacement of the complex. The $\varepsilon_{Nd}(t)$ values show a narrow variation from $+5.0\pm0.2$ to $+5.7\pm0.2$. Titanite and apatite (from samples KB-0, KB-1 and KB-3) have slightly lower $\varepsilon_{Nd}(t)$ values than eudialytes from the same samples (Fig. 5b).

With Hf concentrations of 1221–1646 ppm and Lu/Hf and Yb/Hf ratios of 0.011–0.014 and 0.074–0.107, analyses yield ^{176}Hf/^{177}Hf isotopic ratios from 0.282797 ± 9 to 0.282806 ± 9 and $\varepsilon_{Hf}(t)$ values from $+8.7\pm0.3$ to $+9.0\pm0.3$ (Fig. 5c). In common with the Nd isotopes, all these analyses show some variation in the ^{176}Lu/^{177}Hf and ^{176}Hf/^{177}Hf ratios, and located along the 370 Ma reference line (Fig. 5c). Therefore, our Sr, Nd and Hf isotopic data (initial Sr isotopes: 0.70339–0.70350; $\varepsilon_{Nd}(t)$ values: $+5.0$ to $+5.7$; $\varepsilon_{Hf}(t)$ values: $+8.7$ to $+9.0$) are closely compatible to the literature data (initial Sr isotopes: 0.7030–0.7043; $\varepsilon_{Nd}(t)$ values: $+1.3$ to $+6.0$; $\varepsilon_{Hf}(t)$ values: $+8.0$ to $+9.0$; Patchett et al., 1981; Kramm et al., 1993; Kramm and Kogarko, 1994; Barfod et al., 2003; Downes et al., 2005; Korgarko et al., 2008; Lahaye et al., 2008a,b).

4.3. Lovozero syenite, Kola Peninsula, Russia

In contrast to eudialytes from Khibiny, those from Lovozero have much higher contents of Sr (10289–17928 ppm), Sm (503–881 ppm)

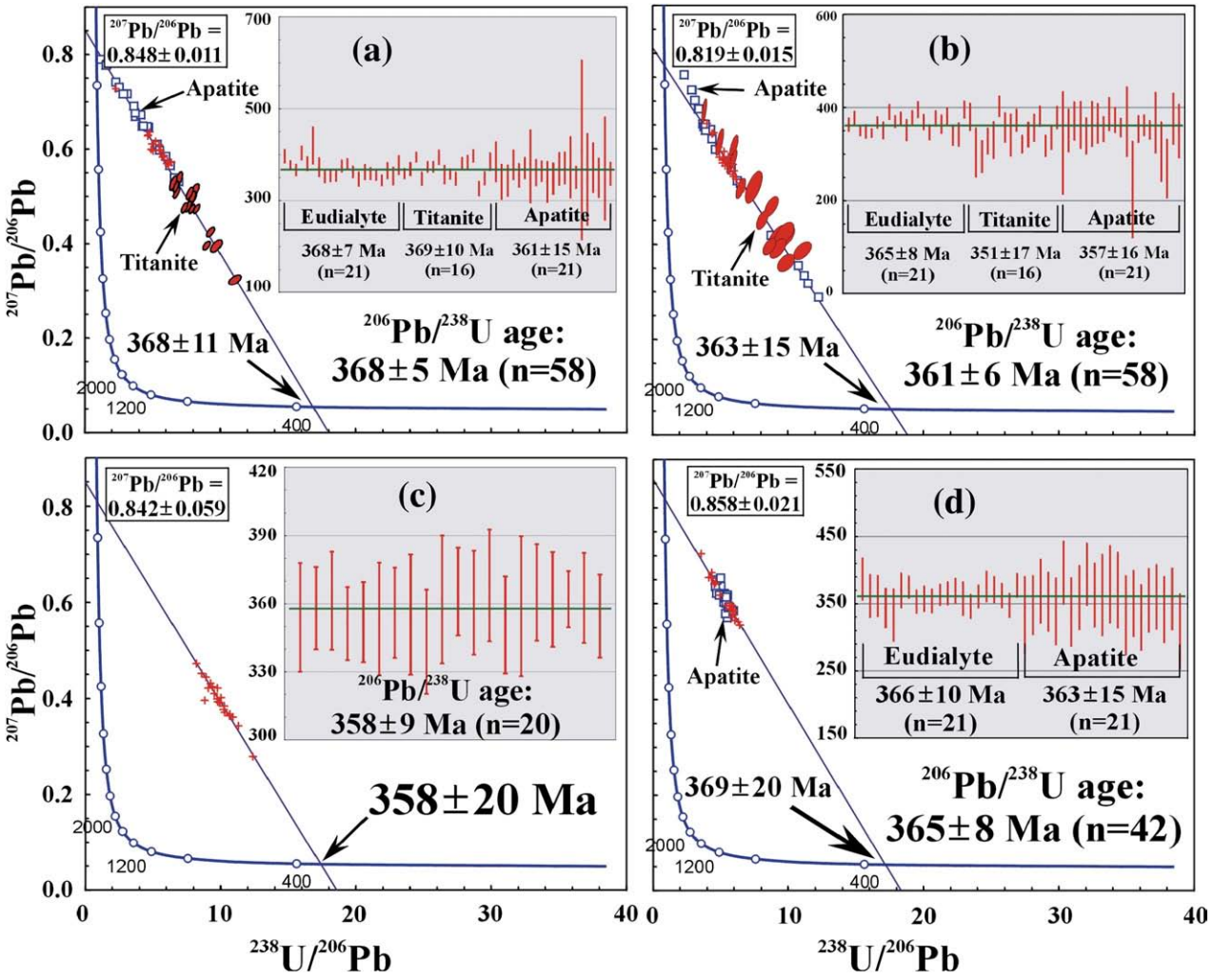

Fig. 4. U–Pb ages and common Pb isotopic composition for eudialyte from the Khibiny complex, Russia. (a) KB-0; (b) KB-1; (c) KB-2 and (d) KB-3.

and Nd (2815–3887 ppm) (Table 2). U–Pb analyses for Lovozero eudialytes yield lower intercept ages from of 357 ± 20 to 377 ± 88 with ^{207}Pb corrected ^{206}Pb/^{238}U ages of 359 ± 8 to 376 ± 6 (Fig. 6). The average ^{207}Pb corrected ^{206}Pb/^{238}U age from the five samples is 370 ± 10 Ma (Fig. 6f), identical to that of Khibiny within analytical errors.

^{87}Sr/^{86}Sr ratios range from 0.70378 ± 1 to 0.70404 ± 1 with ^{87}Rb/^{86}Sr ratios from 0.00208 to 0.00353 (Fig. 7a). ^{143}Nd/^{144}Nd isotopic ratios vary from 0.512662 ± 8 to 0.512739 ± 6 with ^{147}Sm/^{144}Nd ratios from 0.1212 to 0.1641 and $\varepsilon_{Nd}(t)$ values from +3.5 ± 0.1 to +4.1 ± 0.1 (Fig. 7b). ^{176}Hf/^{177}Hf isotopic ratios vary from 0.282741 ± 9 to 0.282790 ± 13 with $\varepsilon_{Hf}(t)$ values from +6.2 ± 0.3 to +8.1 ± 0.5 (Fig. 7c). Therefore, our Sr, Nd and Hf isotopic data are closely compatible to the literature data (initial Sr isotopes: 0.7033–0.7041; $\varepsilon_{Nd}(t)$ values: +2.9 to +4.9; $\varepsilon_{Hf}(t)$ values: +5 to +8; Kramm et al., 1993; Kramm and Kogarko, 1994; Downes et al., 2005; Korgarko et al., 2008; Kogarko et al., 2010; Lahaye et al., 2008a,b).

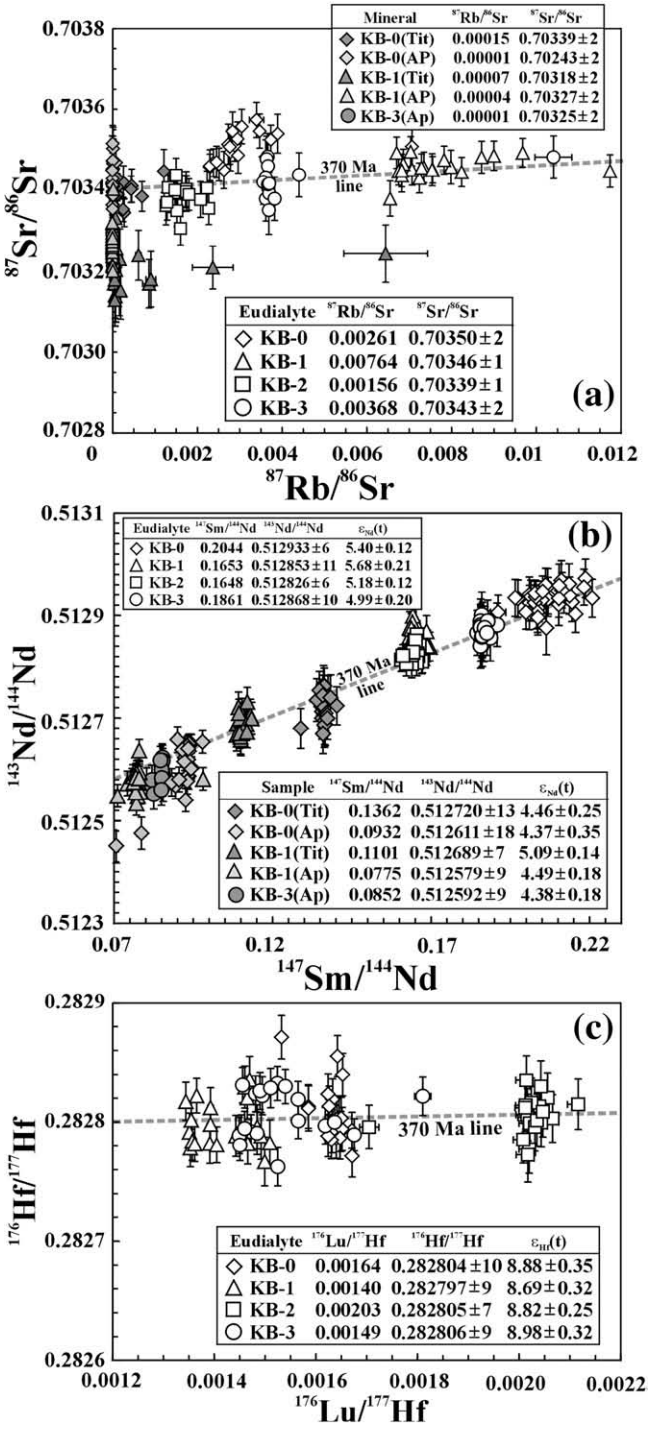

Fig. 5. Sr–Nd–Hf isotopic composition for eudialyte from the Khibiny complex, Russia. (a) Sr isotopic data; (b) Nd isotopic data; and (c) Hf isotopic data.

4.4. Saima syenite, China

In contrast to eudialyte from the Ilímaussaq, Khibiny and Lovozero complexes, the samples from the Saima complex have higher Sr (22514–27323 ppm) and Hf (2235–2510 ppm) (Table 2). In the Tera–Wasserburg U–Pb diagrams, the lower intercept age of sample SM06 is 217 ± 39 Ma with ^{207}Pb corrected ^{206}Pb/^{238}U ages of 220 ± 15 Ma (Fig. 8a). When combined with data for associated titanite, the above two ages are identical at 223 ± 4 Ma (Fig. 8a). Interestingly, sample SM07 shows a large range of Pb isotopic variations, which yield a precise lower intercept age of 224 ± 5 Ma with ^{207}Pb corrected ^{206}Pb/^{238}U ages of 224 ± 4 Ma (Fig. 8b). Both ages are identical to the zircon U–Pb age of 225 ± 1 Ma, obtained from the nearby eudialyte-free nepheline syenite (Wu, unpublished data). Sample SM25 gives a younger lower intercept age of 193 ± 4 Ma with ^{207}Pb corrected ^{206}Pb/^{238}U ages of 193 ± 3 Ma (Fig. 8c). This young age is considered to result from Pb loss, which is supported by a petrographically observed alteration (see Appendix A).

Rb/Sr ratios vary between 0.00023 and 0.00027, ^{87}Sr/^{86}Sr ratios vary in a narrow range from 0.70854 ± 3 to 0.70857 ± 2 (Fig. 8d), consistent with previously reported whole-rock data (Jing et al., 1995; Chen, 1996; Zhou et al., 1996). The $\varepsilon_{Nd}(t)$ values range from −12.3 ± 0.2 to −12.7 ± 0.2 (Fig. 8e). In addition, titanite from SM06 yields similar Sr–Nd isotopic data. The $\varepsilon_{Hf}(t)$ values range from −11.4 ± 0.3 to −10.4 ± 0.4 (Fig. 8f). In contrast to the Ilímaussaq and Khibiny samples, there are less significant Sr–Nd isotopic variations among the eudialytes from different samples, suggesting that alteration did not modify the Sr–Nd–Hf isotopic systems.

4.5. Tamazeght complex, Morocco

U–Pb analyses of Tamazeght eudialytes yield lower intercept ages of 39 ± 9 Ma for TM177, 50 ± 105 Ma for TM241 and 46 ± 95 Ma for TMZ298 in the Tera–Wasserburg diagrams (Fig. 9), with ^{207}Pb corrected ^{206}Pb/^{238}U ages of 40 ± 5, 43 ± 35, and 43 ± 24 Ma (Fig. 9a, b, c). The latter two ages are highly imprecise due to the low amounts of radiogenic Pb, but still agree with the age of ~44 Ma (Marks et al., 2008a,b). Eudialytes from this complex have high Sr concentrations of 14132–25699 ppm with Rb/Sr ratios of 0.0006–0.0019 and the ^{87}Sr/^{86}Sr ratios range from 0.70320 ± 2 to 0.70326 ± 3 (Fig. 9d), only slightly lower than 0.7033–0.7035 obtained by Marks et al. (2009) from whole-rock data of other samples in the complex. The eudialytes have $\varepsilon_{Nd}(t)$ values between +4.0 ± 0.1 and +4.6 ± 0.3 (Fig. 9e), slightly higher than +2.0–+4.1 obtained by Marks et al. (2009) from whole-rock analyses. The obtained $\varepsilon_{Hf}(t)$ values vary from +4.5 ± 0.2 to +5.9 ± 0.3 (Fig. 9f).

4.6. Mont Saint Hilaire, Canada

In the Tera–Wasserburg U–Pb diagram (Fig. 10a, b), the lower intercept ages are 137 ± 35 (MSH38) and 137 ± 60 (MSH58) Ma, with ^{207}Pb corrected ^{206}Pb/^{238}U ages of 128 ± 12 (MSH38) and 132 ± 16 (MSH52) Ma. These ages are identical to the zircon age of 141 ± 7 Ma reported by Cox and Wilton (2006). In common with the Ilímaussaq complex, eudialyte from MSH52 has a high Rb/Sr ratio of 0.14, making *in situ* laser ablation analysis impossible. However, for MSH38, the ^{87}Rb/^{86}Rb and ^{87}Sr/^{86}Sr isotopic ratios are 0.00580 and 0.70385 ± 3 (Fig. 11a), comparable to the whole-rock data (Currie et al., 1986). The $\varepsilon_{Nd}(t)$ values for the two eudialytes are +4.4 ± 0.2 and +5.0 ± 0.1 and the $\varepsilon_{Hf}(t)$ values are +11.6 ± 0.5 and +8.4 ± 0.5, respectively (Fig. 11b, c).

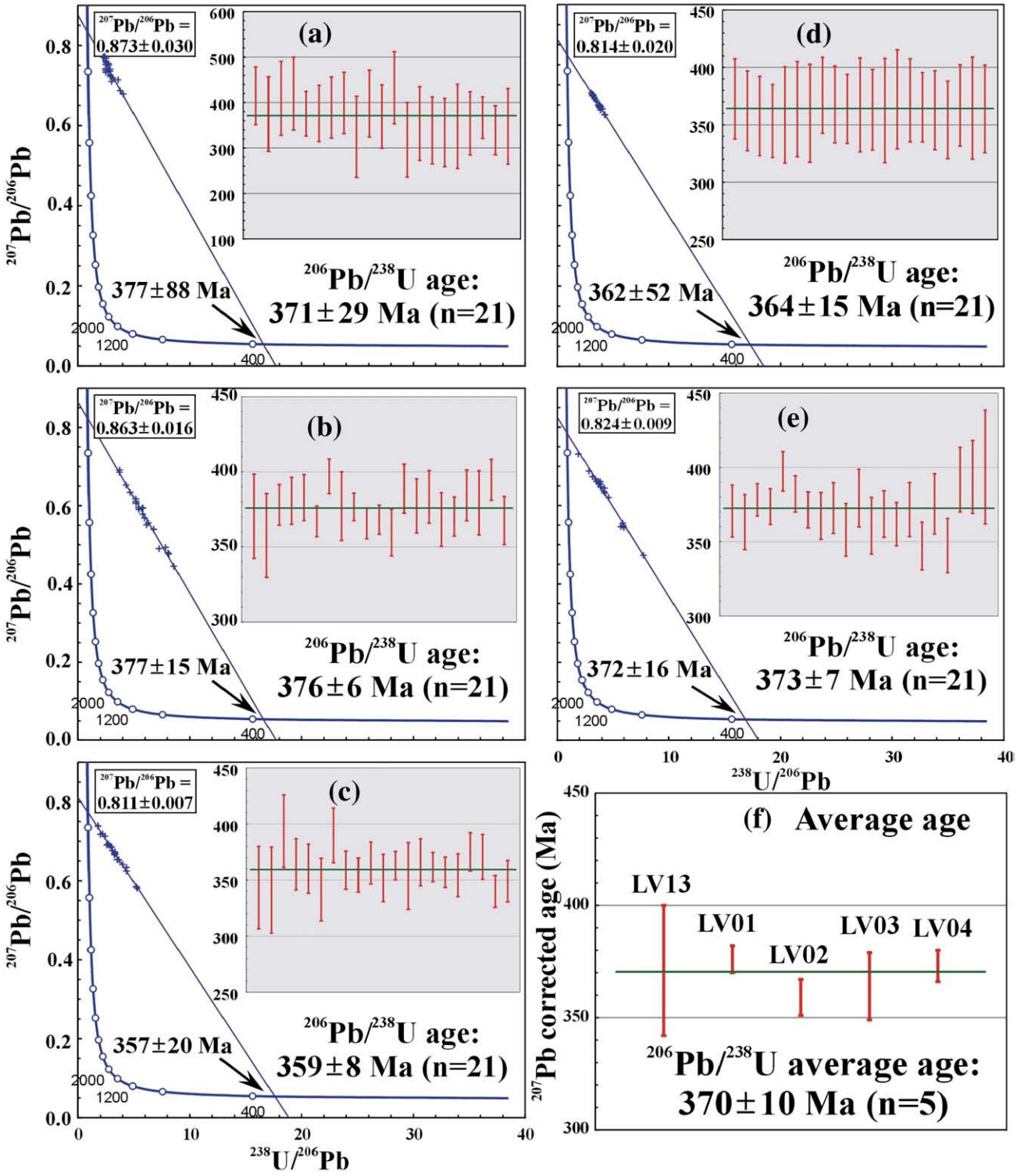

Fig. 6. U–Pb ages and common Pb isotopic composition for eudialyte from the Lovozero complex in Kola of Russia. (a) LV13; (b) LV01; (c) LV02; (d) LV03, (e) LV04 and (f) average age of the above five samples.

4.7. Other localities

4.7.1. Poços de Caldas

Due to high common lead contents, eudialyte (PDC) from this locality yield an imprecise lower intercept age of 78 ± 23 Ma. The ^{207}Pb corrected $^{206}Pb/^{238}U$ age is 77 ± 13 Ma (Fig. 12a). The Rb/Sr and Lu/Hf ratios are of 0.002 and 0.007, respectively. The $^{87}Rb/^{86}Rb$, $^{87}Sr/^{86}Sr$, $^{147}Sm/^{144}Nd$, $^{143}Nd/^{144}Nd$, $^{176}Lu/^{177}Hf$ and $^{176}Hf/^{177}Hf$ isotopic ratios are 0.00457, 0.70529 ± 2, 0.0851, 0.512413 ± 6, 0.0025, and 0.282653 ± 11, with $\varepsilon_{Nd}(t)$ and $\varepsilon_{Hf}(t)$ values of −3.3 ± 0.2 and −2.5 ± 0.4 (Fig. 12 d, e, f), in which the Sr–Nd isotopic data are comparable to the associated nepheline syenites (Shea, 1992).

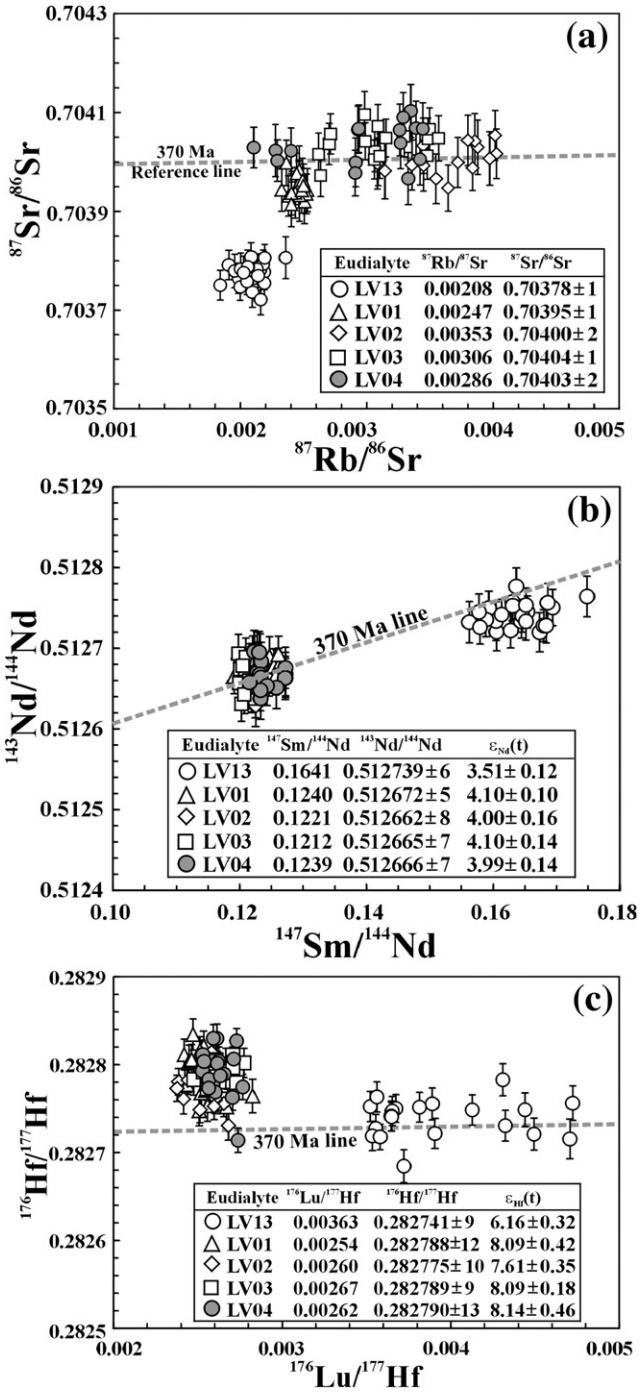

Fig. 7. Sr–Nd–Hf isotopic composition for eudialyte from the Lovozero complex, Kola, Russia. (a) Sr isotopic data; (b) Nd isotopic data; and (c) Hf isotopic data.

4.7.2. Kipawa

In the Tera–Wasserburg U–Pb diagram (Fig. 12b), the lower intercept ages are 1014 ± 61 Ma, with ^{207}Pb corrected $^{206}Pb/^{238}U$ ages of 1012 ± 16 Ma for eudialyte (KPW) from this locality. The high Rb/Sr ratio of 0.03 makes *in situ* laser ablation analysis impossible. The sample has an average Lu content of 577 ppm, which corresponds to a $^{176}Lu/^{177}Hf$ ratio of ~0.04; much higher than those of other samples and making accurate measurement of the $^{176}Hf/^{177}Hf$ impossible by laser ablation techniques. Using a 120 μm spot size, the $^{147}Sm/^{144}Nd$ and $^{143}Nd/^{144}Nd$ isotopic ratios are 0.2438 and 0.512403 ± 6, with $\varepsilon_{Nd}(t)$ value of 10.6 ± 0.1 (Fig. 12e). However, this eudialyte shows some Sm/Nd isotopic variations, which yield an imprecise isochron with age of 965 ± 75 Ma (Fig. 12e), identical to the U–Pb age within analytical errors. Solution analysis of this sample gives an $\varepsilon_{Hf}(t)$ value of −6.1 ± 0.1 and a $\varepsilon_{Nd}(t)$ value of −9.9 ± 0.1, the latter of which is similar to that obtained by laser ablation.

4.7.3. Langesund Fjord, Norway

Because of its high common lead contents (472 ppm Pb), this sample (LGS) cannot be used to obtain reasonable U–Pb ages (Fig. 12c). However, the apatite from this sample exhibits considerable Pb isotopic variations, which yield a lower intercept age of 261 ± 6 Ma, with ^{207}Pb corrected $^{206}Pb/^{238}U$ ages of 260 ± 4 Ma Fig. 12c). This age is in accord with the age data of Corfu and Dahlgren (2008) and Larsen et al. (2008).

In contrast to other complexes, eudialyte from this sample has a Sr content of 2409 ppm, and the high REE concentrations, hence significant interference, makes the Sr isotopic determination by laser methods impossible (see below). Using a 120 μm spot size, the $^{147}Sm/^{144}Nd$, $^{143}Nd/^{144}Nd$, $^{176}Lu/^{177}Hf$ and $^{176}Hf/^{177}Hf$ isotopic ratios are 0.0847, 0.512610 ± 6, 0.00246 and 0.282833 ± 7, with $\varepsilon_{Nd}(t)$ and $\varepsilon_{Hf}(t)$ values of +3.2 ± 0.1 and +7.5 ± 0.3 (Fig. 12f). Apatite from this sample gives $^{87}Rb/^{86}Rb$, $^{87}Sr/^{86}Sr$, $^{147}Sm/^{144}Nd$ and $^{143}Nd/^{144}Nd$ isotopic ratios are 0.00029, 0.70366 ± 2, 0.0913 and 0.512667 ± 18, with $\varepsilon_{Nd}(t)$ value of +4.1 ± 0.4 (Fig. 12d). These Sr–Nd–Hf isotopic data are closely consistent to those reported for the hosted Larvik batholith (Neumann et al., 1988; Rasmussen et al., 1988; Dahlgren et al., 1996). For example, zircon $\varepsilon_{Hf}(t)$ values of +6.7 to +5.5 by Dahlgren et al. (1996) from the Larvik batholith are excellently coincided with the present data.

5. Discussion

5.1. Compositional variation of eudialyte

Data obtained in this study by laser ablation method permit comparisons of the trace element and isotopic composition of eudialyte from diverse localities. Fig. 13 shows that the distribution pattern of REE and other trace elements obtained in present study, three subgroups of eudialyte exist (Fig. 13). In common with their host rocks (Kramm and Kogarko, 1994; Tan et al., 1999; Arzamastsev et al., 2001, 2005), eudialytes from Khibiny, Lovozero and Saima have relatively low REE concentrations with no significant Eu and Sr anomalies (i.e. the high Sr subgroup in Fig. 13a, b). Eudialyte from the Lovozero has the highest REE contents with weak positive Eu anomalies. In contrast, eudialytes from Ilímaussaq, Mont Saint Hilaire, Kipawa and Langesund Fjord display well-defined negative Eu anomalies coupled with Sr depletion (i.e. the low Sr subgroup on Fig. 13c, d), Similar features are evident in the host rocks (Bailey et al., 2001, 2006; Sørensen et al., 2006). Eudialyte from the Tamazeght complex contains much less REE (i.e. the low REE subgroup in Fig. 13e, f). These groups suggest that eudialyte-bearing agpaitic rocks might have diverse origins and/or petrogenetic processes.

5.2. Eudialyte: potential for the U–Pb age determination of agpaitic rocks

U–Pb isotopic dating of zircon and baddeleyite is one of the most important methods for determining the age of emplacement of plutonic rocks as these minerals have high U contents, low amounts of common Pb, and high closure temperatures. However, this method cannot be typically used for the agpaitic rocks as Zr is highly soluble in this type of magma, precluding the crystallization of zircon and/or baddeleyite. Thus, agpaitic rocks are characterized by occurrence of the zirconium-rich minerals such as eudialyte and låvenite etc. To date the potential of eudialyte as a U–Pb geochronometer has not been investigated.

According to our study, eudialyte has U concentrations of 16–1249 ppm (Fig. 14a), which make it possible to determine precisely

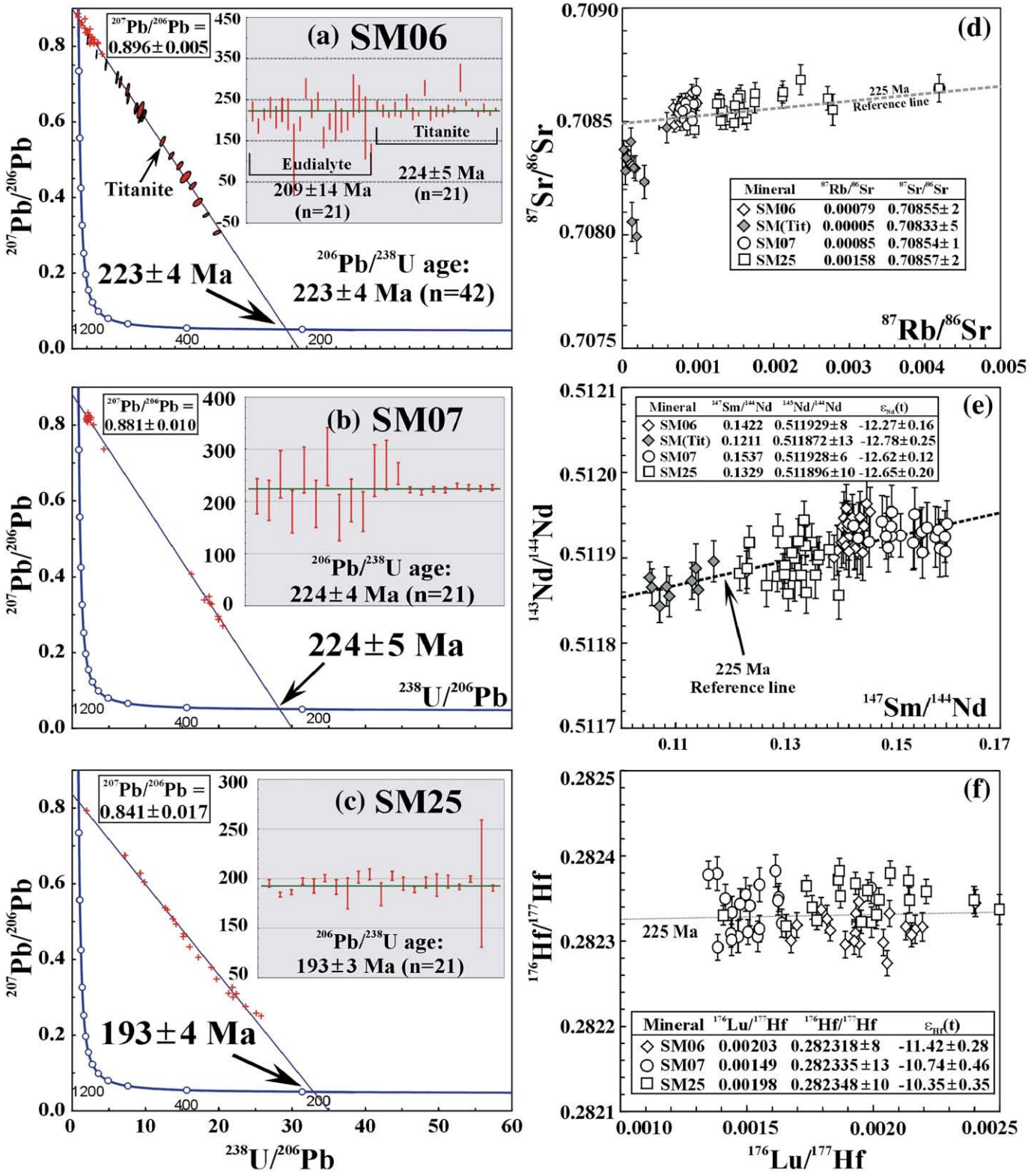

Fig. 8. U–Pb ages, common Pb and Sr–Nd–Hf isotopic composition for eudialyte from the Saima complex in northeastern China. (a) SM06 (U–Pb); (b) SM07 (U–Pb); (c) SM25 (U–Pb); (d) Sr isotopic data; (e) Nd isotopic data; and (f) Hf isotopic data.

the U–Pb isotope composition, by either traditional TIMS or modern *in situ* techniques. However, several factors have to be considered if this mineral is to be used for geochronology. First, eudialyte is usually altered and replaced by secondary zircon, baddeleyite, catapleiite, zirsinalite, steenstrupine, wohlerite, mosandrite and other minerals (e.g., Coulson and Chambers, 1996; Coulson, 1997; Sørensen, 1997; Mitchell and Liferovich, 2006). In our studied samples, most eudialytes display only minor alteration. For example in sample

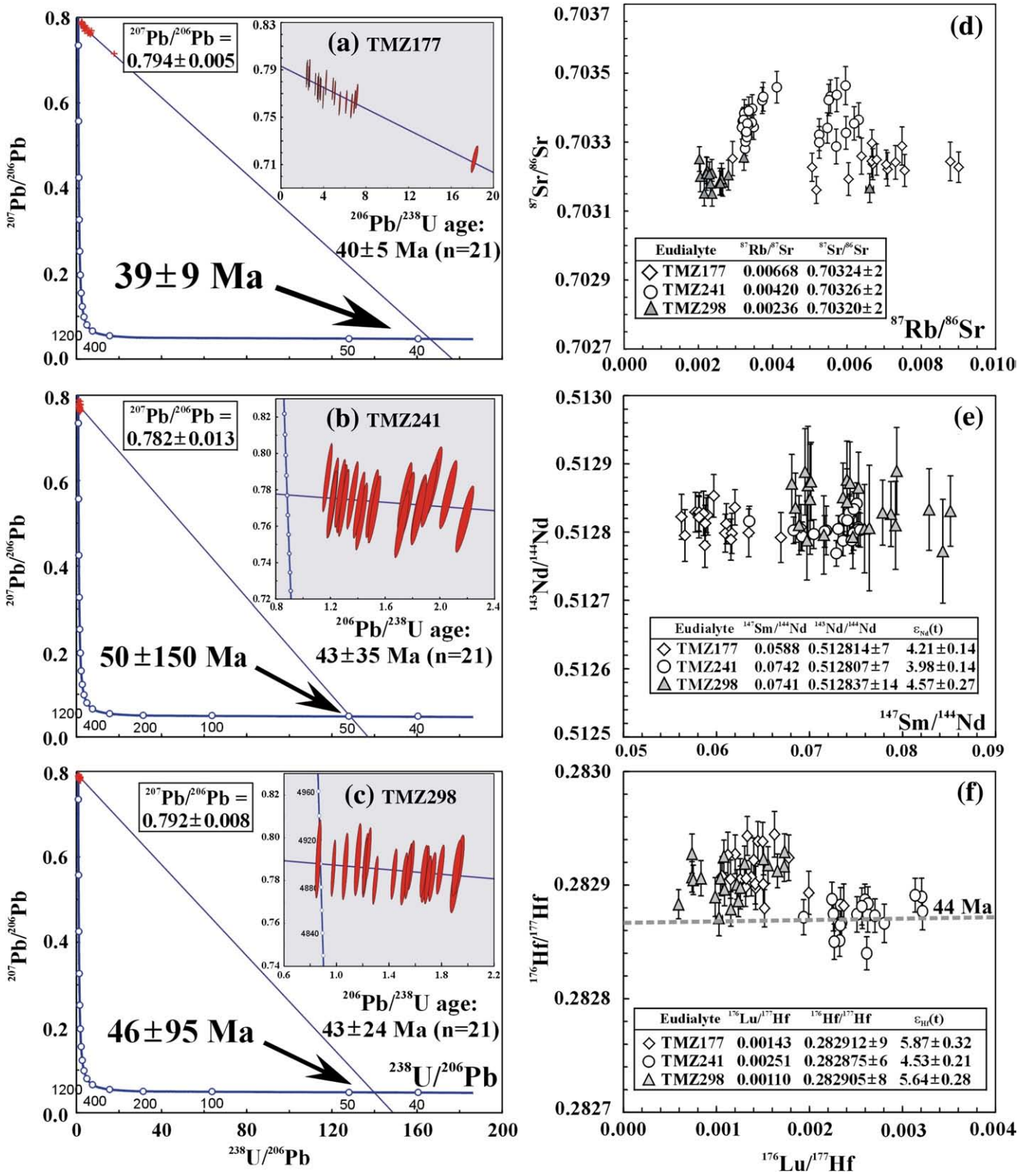

Fig. 9. U–Pb ages, common Pb and Sr–Nd–Hf isotopic composition for eudialyte from the Tamazeght complex in Morocco. (a) TMZ177 (U–Pb); (b) TMZ241 (U–Pb); (c) TMZ298 (U–Pb); (d) Sr isotopic data; (e) Nd isotopic data; and (f) Hf isotopic data.

LV13 from Lovozero, the eudialyte occurs as large euhedral crystals with oscillatory zoning, suggesting this is a primary feature of crystallization from magma (Kogarko et al., 1982; Sørensen, 1997). However, some grains of eudialyte from the Ilímaussaq, Saima and Mont Saint Hilaire complexes have been altered along grain boundaries and fractures. Therefore, detailed petrographic observations are necessary before laser analyses, which also imply that *in situ* technique is the best method for U–Pb isotopic analyses.

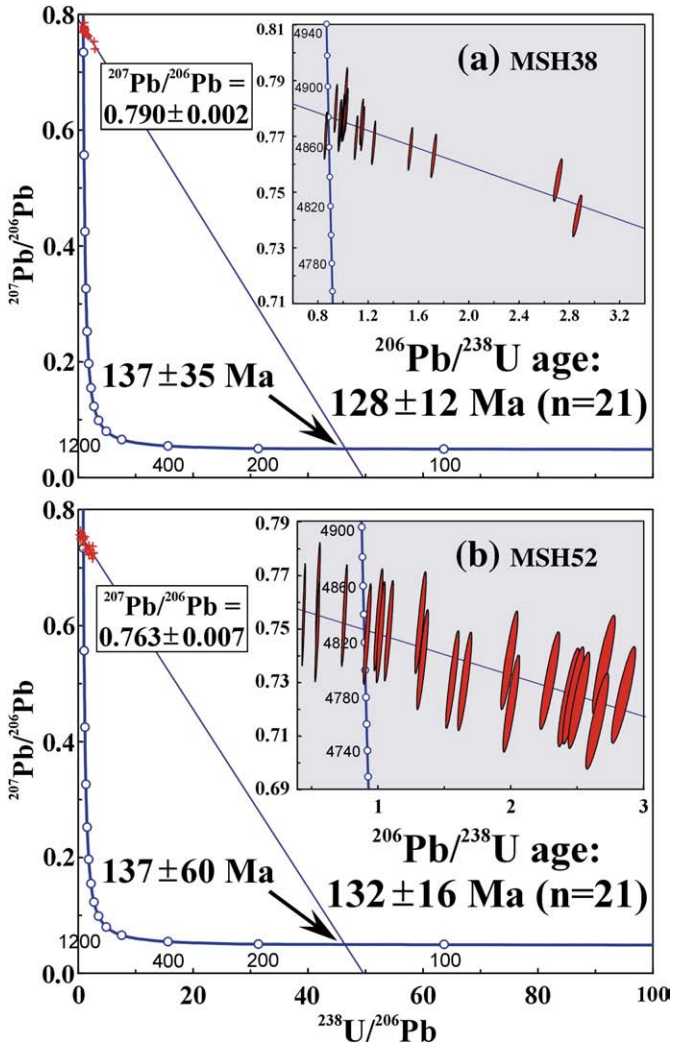

Fig. 10. U–Pb ages and common Pb isotopic composition for eudialyte from the Mont Saint Hilaire, Quebec, Canada. (a) MSH38; and (b) MSH52.

A second problem is with regard to is the eudialyte U–Pb closure temperature. It is commonly accepted that eudialyte is of primarily magmatic origin with crystallization temperature of ~860–720 °C (Kogarko et al., 1982; Sørensen, 1997), which is supported by its euhedral habit, (Coulson and Chambers, 1996; Coulson, 1997; Pfaff et al., 2008). However, it is also known that eudialyte can be formed during the hydrothermal stage of agpaitic magma evolution at temperatures of <350 °C (e.g., Olivo and Williams-Jones, 1999; Schilling et al., 2009). Moreover, petrographic observations have indicated that this mineral is susceptible to alteration in the later stage of evolution of agpaitic magmas (Olivo and Williams-Jones, 1999; Salvi et al., 2000; Mitchell and Liferovich, 2006; Sørensen, 2006); such alteration could disturb and reset the original U–Pb isotopic system.

In order to understand fully the U–Pb closure temperature of eudialyte, a theoretical calculation is illustrated Fig. 15. The kinetic-porosity model of Zhao and Zheng (2007) is applied for the calculation of diffusion coefficients, and the method of Dodson (1973) is used for calculation of the closure temperatures (Tc). For comparison, the diffusion coefficients and closure temperatures of zircon and titanite are also included. From these data it is apparent that eudialyte has much more rapid Pb diffusion rate and lower closure temperatures than either zircon or titanite (Fig. 15). Assuming a cooling rate of 100 °C/Ma, a eudialyte of 10 mm grain-size (typical size of material used in this study) has a U–Pb closure temperature of ~675 °C, much lower than that of zircon and titanite of the same size (Fig. 15b). However, in our samples, the analysed titanite has commonly a grain-size of only ~100 μm, which has a calculated Pb closure temperature of ~740 °C at a cooling rate of 100 °C/Ma, *i.e.* slightly higher than that (~700 °C) estimated by Frost et al. (2000), and not very different from that of eudialyte if a ~50 °C error is considered.

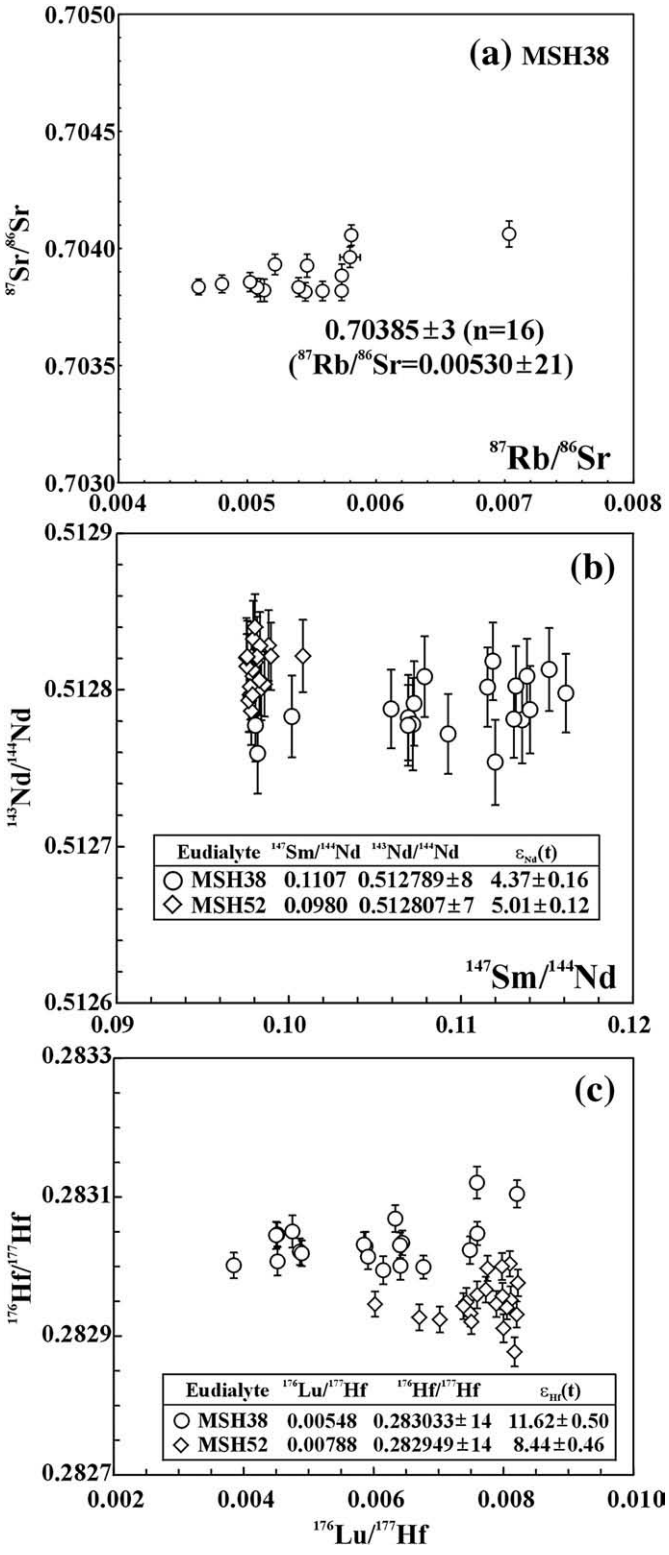

Fig. 11. Sr–Nd–Hf isotopic composition for eudialyte from the Mont Saint Hilaire, Quebec, Canada. (a) Sr isotopic data; (b) Nd isotopic data; and (c) Hf isotopic data.

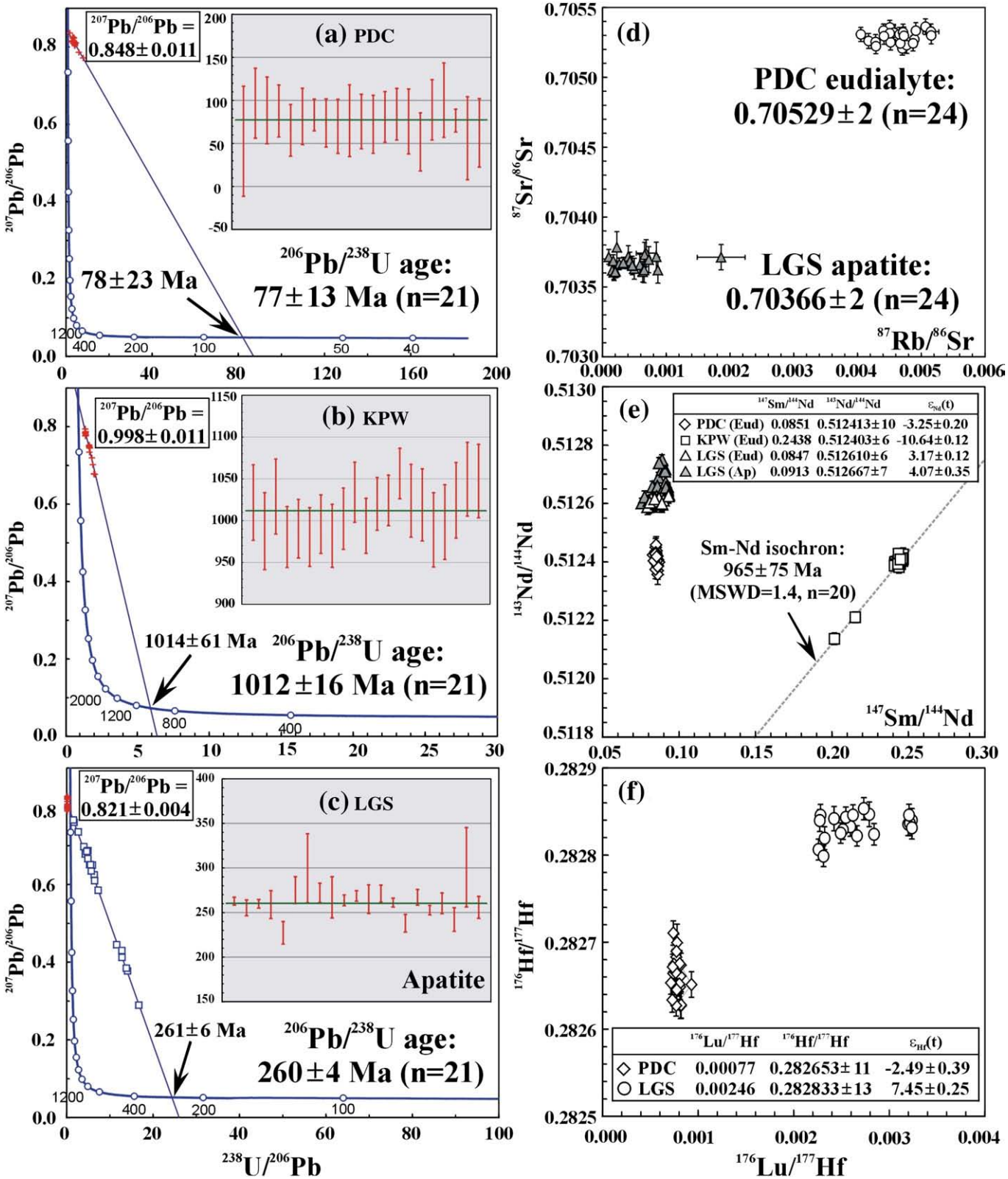

Fig. 12. U–Pb ages, common Pb and Sr–Nd–Hf isotopic composition for eudialyte from the Poços de Caldas (PDC), Brazil, Kipawa (KPW), Quebec, Canada, and Langesund Fjorden (LGS), Norway. (a) PDC (U–Pb); (b) KPW (U–Pb); (c) LGS (U–Pb); (d) Sr isotopic data; (e) Nd isotopic data; and (f) Hf isotopic data.

Finally, we have to consider the composition of common Pb. As shown in this study (Fig. 14b), eudialytes have varying common Pb contents with most ranging from 60 to 100% of the total Pb. This results in the analyses lying on a chord to Concordia. In such a situation the lower intercept of this discordia line can be considered as the U–Pb age. If there is a datum near the lower intercept, it is possible to obtain a precise age e.g. as shown by

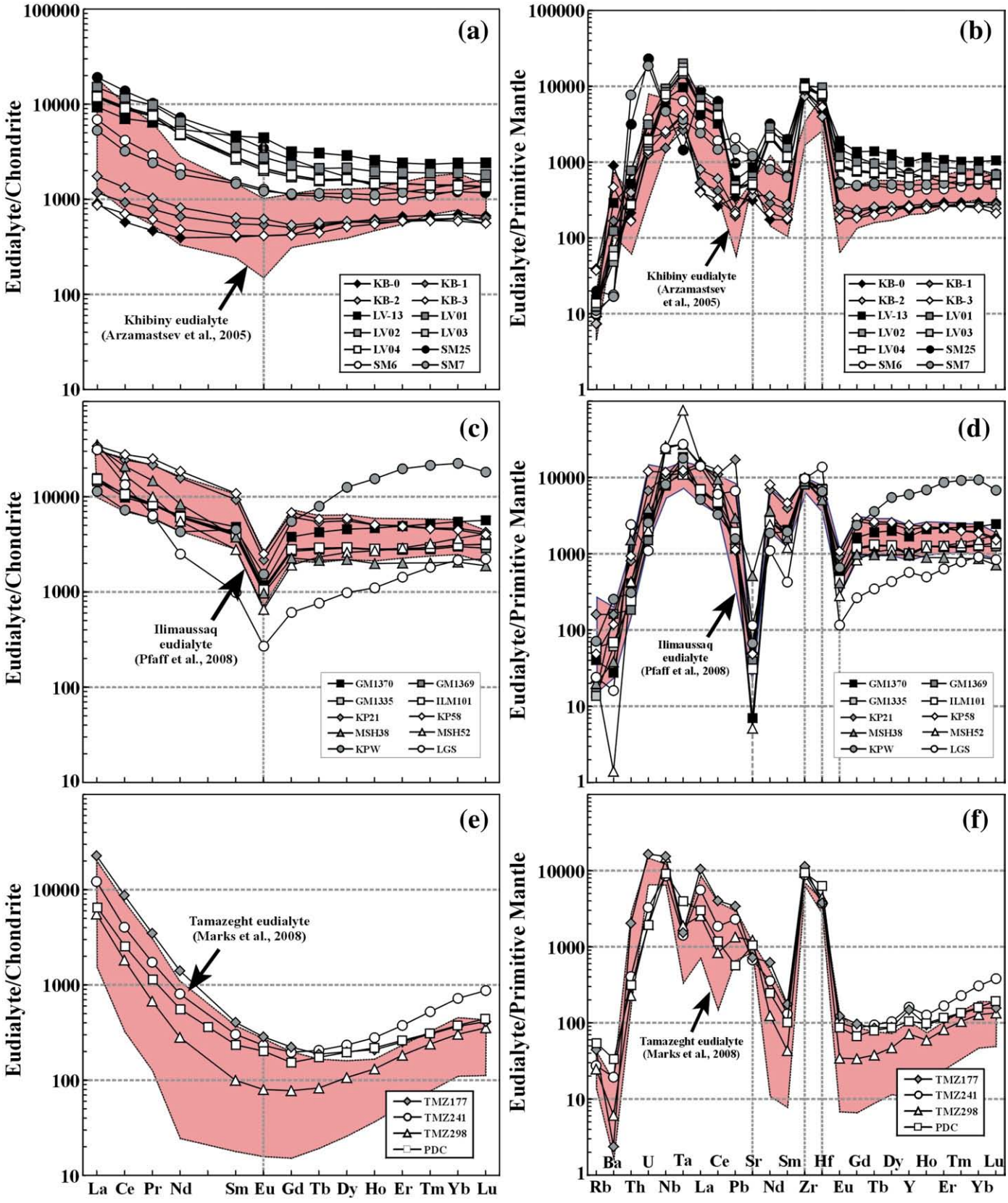

Fig. 13. REE patterns and spidergrams of eudialytes. Three subgroups can be identified, i.e., (a and b) high Sr, (c and d) low Sr and (e and f) low REE. The fields of Khibiny, Ilímaussaq and Tamazeght eudialytes are from Arzamastsev et al. (2005), Pfaff et al. (2008) and Marks et al. (2008b).

sample SM07 (Fig. 8c). Alternatively, a ^{207}Pb correction is applied to calculate the weighted $^{206}Pb/^{238}U$ age assuming that there has been no Pb loss (Williams, 1998). In this case, the age precision and accuracy depend on the common Pb composition which is generally determined using the theoretical two-stage model of Stacey and Kramers (1975). Typically this is appropriate for zircon and baddeleyite age determination as their

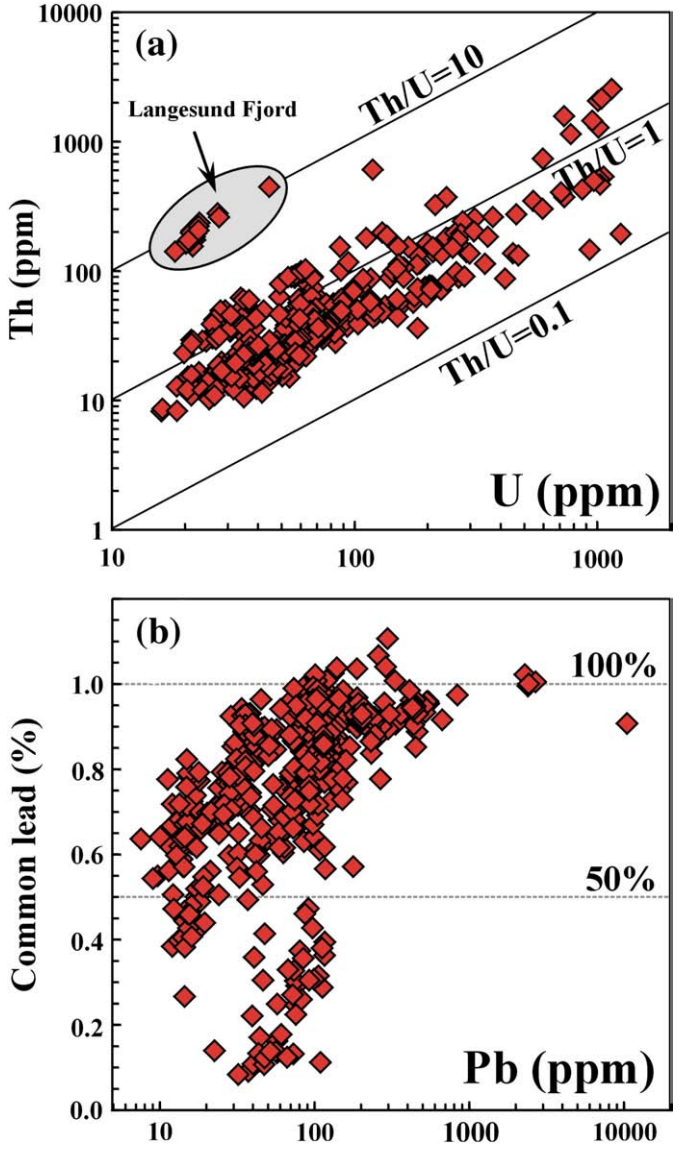

Fig. 14. U, Th and Pb concentrations (a) and percentage of common Pb (b) of eudialytes.

common Pb content is low. In this study, most of our analysed eudialyte data are located in the upper half of the discordia chord and, the two-stage model is not applicable. Therefore, a datum with low common Pb is necessary for determination of the precise composition of common lead. According to the petrographic observations, titanite and apatite always occur in close association with eudialyte, and are considered to have crystallized contemporaneously. Considering that the agpaitic magma generally has a rapid cooling history, and hence the constituting minerals have an identical crystallization age (Markl et al., 2001; Féménias et al., 2005; Krumrei et al., 2006), we suggest, therefore, that titanite and apatite (if present) may be used to construct the above discordia chord. In the sample KB-0, eudialyte defines a discordant chord with a common $^{207}Pb/^{206}Pb$ ratio of 0.834 ± 0.024 and lower intercept ^{207}Pb corrected $^{206}Pb/^{238}U$ ages of 354 ± 27 and 356 ± 11 Ma. However, these data combined with those for titanite and apatite, give a common $^{207}Pb/^{206}Pb$ ratio of 0.848 ± 0.011 and the lower intercept age is 368 ± 11 Ma (Fig. 4a). If this common lead composition is applied, the ^{207}Pb corrected $^{206}Pb/^{238}U$ age for this eudialyte is 368 ± 5 Ma, *i.e.* more precise than that (356 ± 11 Ma) obtained by applying the common lead composition as defined by the eudialyte itself (Fig. 4a). With respect to sample SM06, the eudialyte itself yields the lower intercept and ^{207}Pb corrected $^{206}Pb/^{238}U$ ages of 217 ± 39 and 220 ± 15 Ma. However, if the analyses of eudialyte and titanite are combined, the ages are identical as 223 ± 4 Ma (Fig. 8a), and more precise than the ages determined from eudialyte alone. Therefore, a datum with low common Pb is vital for obtaining a precise age for eudialyte.

5.3. Potential of in situ isotopic analysis of eudialyte

Not all minerals can be isotopically measured using *in situ* LA-MC-ICP-MS due to limitations relating to element concentrations and potential interferences. Only those minerals with high concentrations of Sr, Nd and Hf can be used for the determination of Sr, Nd and Hf isotopic compositions with reasonable analytical precision. This limitation raises the question of what elemental concentrations are required for *in situ* Sr, Nd and Hf isotopic ratio determinations that are accurate enough for petrogenetic purposes. With regard to Sr isotopes, two pre-conditions have to be met for highly accurate and precise data; high Sr concentration and low Rb/Sr ratio. The former is necessary for the instrument to yield enough signal intensity, and then high analytical precision, and the latter is needed to avoid interference of ^{87}Rb on ^{87}Sr. According to our work, ~500 ppm of Sr is enough to yield data with a high precision of ± 0.0001 if a large (~140 μm) spot size is used (Fig. 16a). However, a low Rb/Sr ratio is more important than the absolute Sr concentration. In order to evaluate the potential isobaric interference of Rb on Sr isotopes we spiked 200 ppb NBS987 with variable amounts of Rb. The results indicate that samples with Rb/Sr ratios of less than 0.02 ($^{87}Rb/^{86}Sr$–0.05) can be effectively corrected (Yang et al., 2009). In this study, the investigated eudialytes have Rb/Sr ratios from 0.0002 to 0.17 (Fig. 17a), in which some eudialytes from Ilímaussaq (GM1370, KP21, KP58 and ILM101), Mont St. Hilaire (MSH52) and Kipawa (KPW) have Rb/Sr ratios between 0.057 and 0.174; much higher than our Rb/Sr limitation (Table 2). Although three samples (GM1369, GM1335 and LGS) have Rb/Sr ratios lower than our limit, their high HREE concentrations make it impossible to obtain accurate and precise Sr isotopic data. As shown in Fig. 18, Yb/Sr less than 0.1 might be another criterion for *in situ* Sr isotopic analyses of eudialyte. Therefore, not all eudialytes can be analysed by *in situ* laser ablation for their Sr isotopic composition. For suitable samples, the initial $^{87}Sr/^{86}Sr$ ratios calculated from the laser ablation data are consistent with those obtained from solution analysis (Fig. 17b). It is concluded, therefore, that laser ablation of eudialyte can provide reliable Sr isotopic data for petrogenetic purposes.

For Nd isotopic analyses, our previous experiments have shown that the minimum Nd concentration of an ablated subject is approximately 200 ppm using the 50 μm laser spot size (Fig. 16b, Yang et al., 2008). The deviation requirement for practical geological application is $\pm 2\varepsilon$ units, corresponding to a $^{143}Nd/^{144}Nd$ ratio deviation of $+0.0001$. Considering that our analysed eudialytes have Nd contents of up to 25,624 ppm with most of them above 200 ppm (except TMZ298) (Fig. 17c), it is concluded that Nd isotopic compositions can be precisely measured in all eudialytes. Calculated $\varepsilon_{Nd}(t)$ values from the ablation data match well with those obtained by solution analyses (Fig. 17d).

Eudialyte is an ideal mineral for *in situ* Hf isotopic analyses. In this study, the eudialytes analysed have Hf concentrations of 719–4708 ppm (Fig. 17e), which are about 5 times less than those of zircon and baddeleyite. Fortunately, we can use a larger spot size to obtain a high signal intensity as the eudialytes analysed are large (mm to cm). For an average Hf concentration of 2000 ppm, 100–120 μm laser spot size is required if a precision of ± 0.00002 is expected (Fig. 16c). However, Hf isotopic analysis also requires low Lu and Yb contents for isotopic composition determinations due to interferences from ^{176}Lu and ^{176}Yb on ^{176}Hf. Generally, the interference of ^{176}Lu to ^{176}Hf is small and can be accurately corrected, as most of our eudialytes have Lu/Hf ratios<0.08 (which corresponds to $^{176}Lu/^{177}Hf = 0.01$ and $^{176}Yb/^{177}Hf = 0.4$–0.5). The ^{176}Lu correction on ^{176}Hf fails in cases such as the KPW eudialyte as its Lu concentration is much higher than other samples with Lu/Hf ratio of 0.2842 (Fig. 17e). Regarding the interference of ^{176}Yb on ^{176}Hf, it has been demonstrated that our analytical procedure can be effectively applied to zircons with $^{176}Yb/^{177}Hf$ up to 0.4 (Wu et al., 2006). For sample GM1370

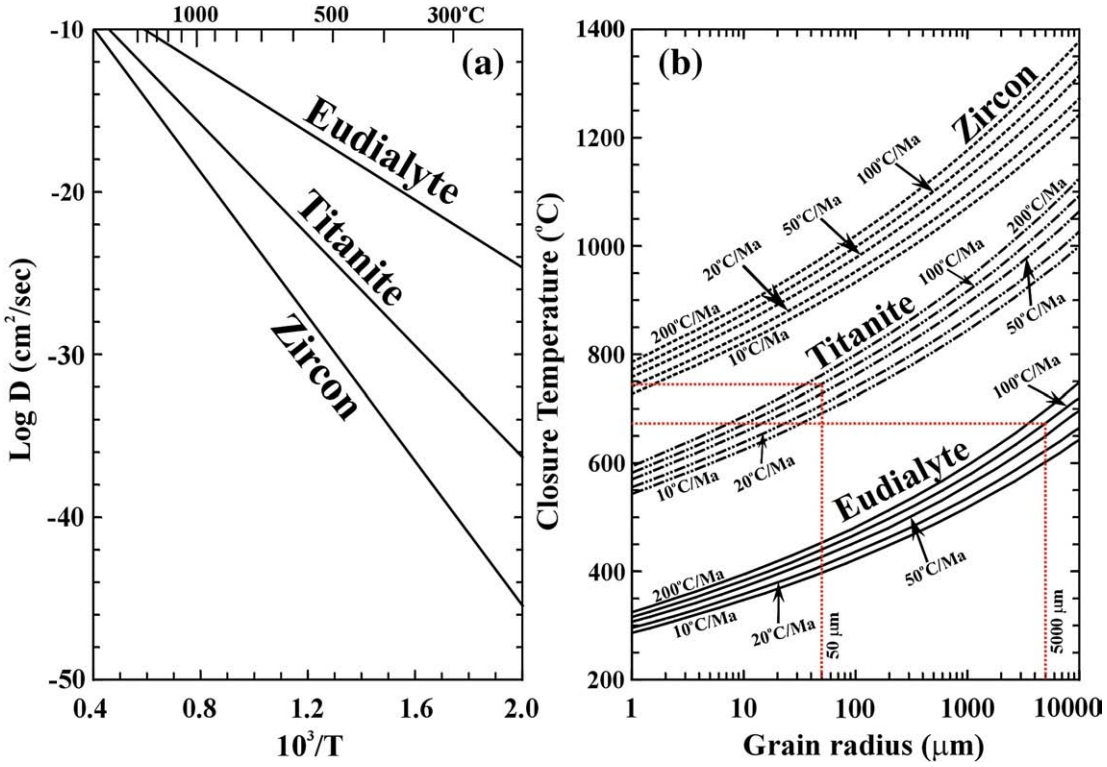

Fig. 15. Theoretical calculation of Pb closure temperature of eudialyte based on the methods of Dodson (1973) and Zhao and Zheng (2007). It is noted that eudialyte has a Pb closure temperature of ~485–695 °C for the grain with size of 1–10 mm at the cooling rates of 10–200 °C/Ma, much lower than that of zircon. However, this temperature is comparable to that of titanite when the latter is one order magnitude smaller of grain-size than eudialyte. The diffusion coefficients of zircon and titanite are from Zhao and Zheng (2007).

(Fig. 3c), which has $^{176}Yb/^{177}Hf$ ratios of 0.236–0.375, the laser analyses yield a $^{176}Hf/^{177}Hf$ ratio of 0.282337 ± 15, identical to the value of 0.282318 ± 5 obtained by solution method (Table 4). However, for the samples KP21, KP58 and KPW, their $^{176}Yb/^{177}Hf$ ratios exceed 0.4 and range up to 1.8–2.2, making it impossible to obtain accurate Hf isotopic compositions using the *in situ* laser ablation technique. Except for the sample MSH52, which has Yb/Hf ratio of ~0.4, the calculated $\varepsilon_{Hf}(t)$ values from laser ablation data are consistent to those obtained by the solution data (Fig. 17f).

In summary, *in situ* laser ablation can provide accurate and precise Sr, Nd and Hf isotopic data for eudialyte which in most instances are identical to data obtained by our solution analyses (Tables 3 and 4,

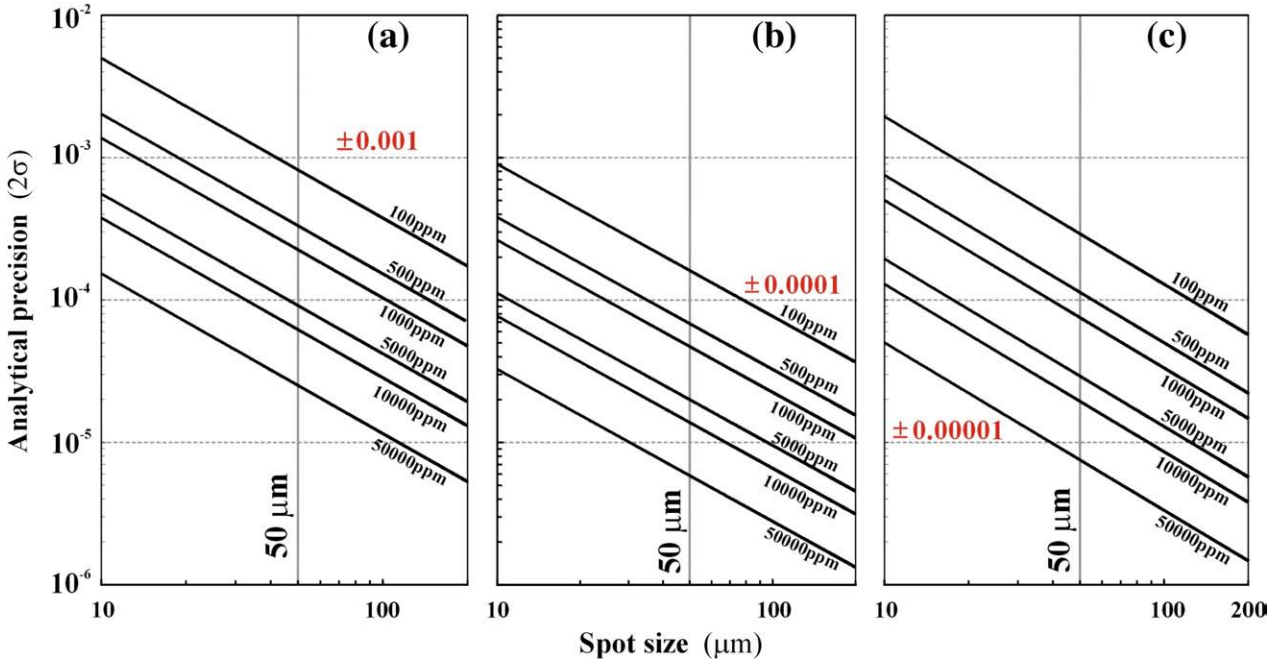

Fig. 16. Relationship between analytical precision of isotopic ratio and spot size during laser ablation analysis. The repetition rate is fixed as 8–10 Hz. (a) Sr isotope, (b) Nd isotope, and (c) Hf isotope.

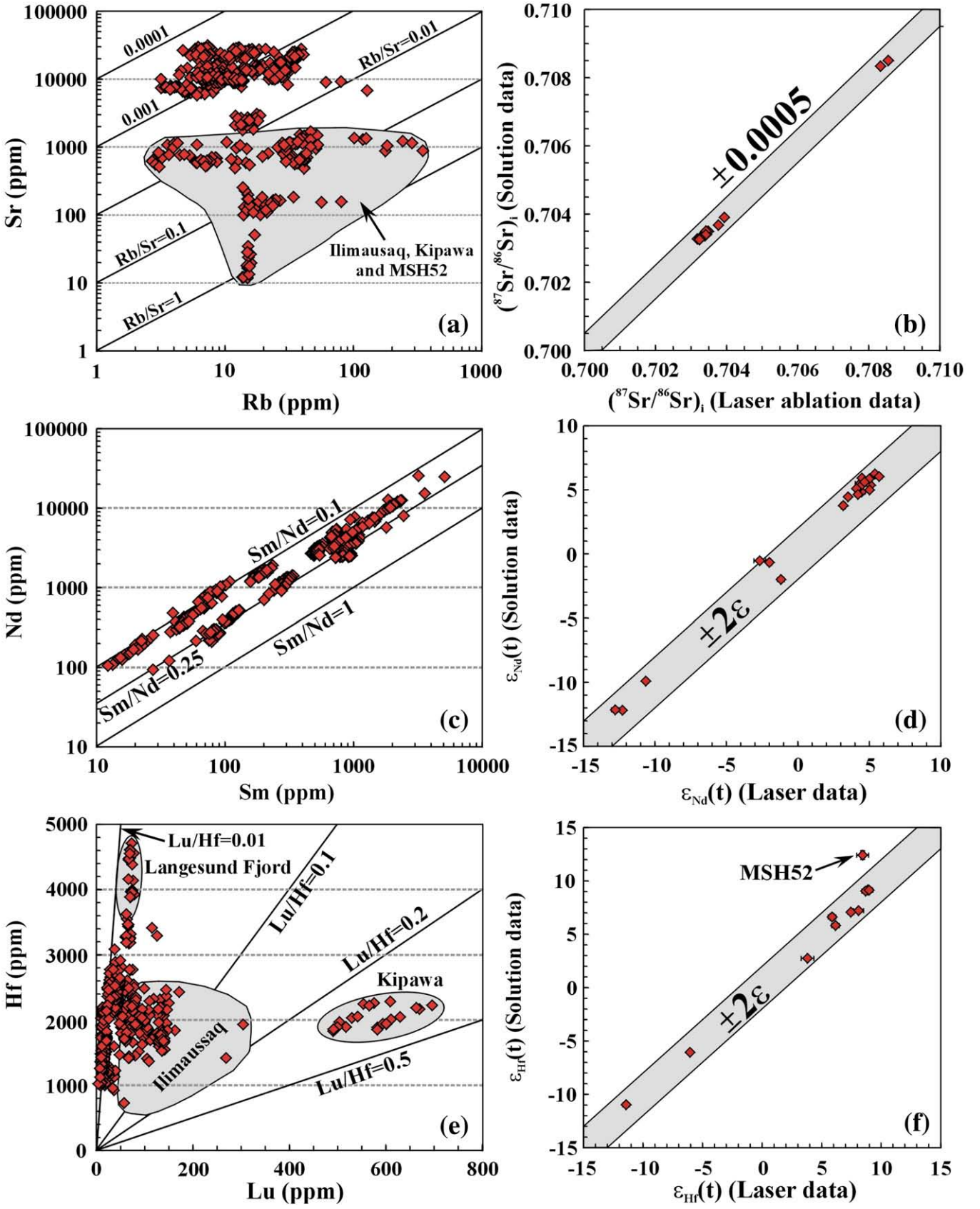

Fig. 17. Elemental variations of Rb–Sr (a), Sm–Nd (b), and Lu–Hf (c) in the eudialytes studied. For suitable samples, the laser ablation results are compared with solution results (b, d and f).

Fig. 17). In our dataset (Table 3), eudialytes from Khibiny, Lovozero, Tamazeght, Mont Saint Hilaire and Langesund Fjord share low $^{87}Sr/^{86}Sr$ (0.7034–0.7038) and high $\varepsilon_{Nd}(t)$ (+3.5 to +5.7) and $\varepsilon_{Hf}(t)$ (+4.5 to +11.6) values (Tables 3 and 4), indicating derivation from depleted mantle. In contrast, eudialytes from Ilímaussaq, Saima, Kipawa and Poços de Caldas show relatively high $^{87}Sr/^{86}Sr$ (>0.705)

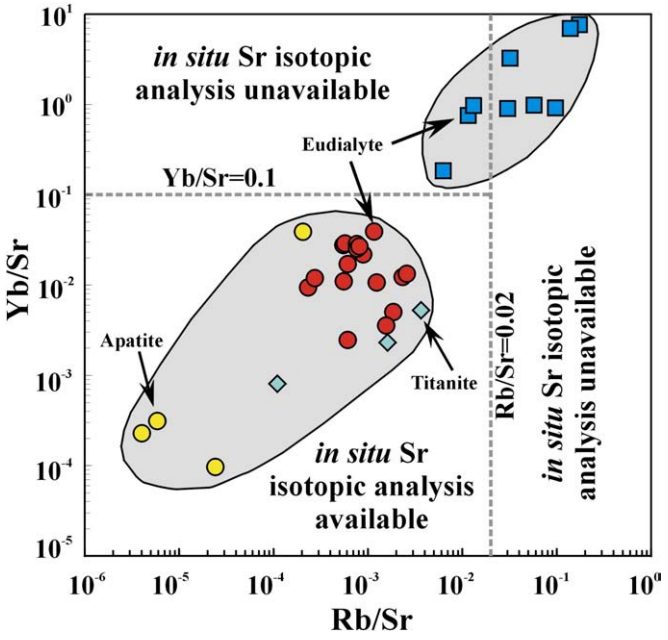

Fig. 18. Rb/Sr and Yb/Sr variation diagram showing possible compositional range for getting accurate Sr isotopic compositions for eudialyte using laser ablation technique.

and low $\varepsilon_{Nd}(t)$ (−1.2 to −12.6) and $\varepsilon_{Hf}(t)$ (+3.0 to +3.8 for Ilímaussaq, −10.7 to −11.4 for Saima and −3.25 for Poços de Caldas) values, implying derivation from enriched lithospheric mantle and/or contaminated by crustal material during their petrogenesis. Thus, the genesis of agpaitic rocks may involve different mantle sources and suggested that crustal contamination might play a significant role for some of the investigated occurrences.

6. Conclusions

Our *in situ* U–Pb, Sr, Nd and Hf analyses of eudialyte lead to the following conclusions:

1) Laser ablation can yield reasonable U–Pb ages for eudialyte group minerals as these have high U and Pb contents. However, precise and accurate determination of the common Pb composition is required if an age with high precision and accuracy is expected;
2) Eudialyte usually contains high contents of Sr, Nd and Hf coupled with low Rb/Sr and Lu/Hf ratios. Laser ablation can yield accurate Sr, Nd and Hf isotopic compositions with high precision. For eudialyte group minerals with low Sr contents, or high Rb/Sr, Yb/Sr and Lu/Hf ratios, it is impossible to obtain Sr and Hf isotopic compositions using the laser ablation technique;
3) Petrographic observation is always necessary for choosing targets for laser ablation as eudialyte always contains inclusions of earlier-crystallized minerals and is commonly altered. Therefore, *in situ* analysis is an ideal method for age determination and isotopic compositions;
4) Analyses of eudialytes from Ilímaussaq, Khibiny, Lovozero, Saima, Tamazeght, Mont Saint Hilaire, Kipawa, Poços de Caldas and Langesund Fjord show a wide range of Sr, Nd and Hf isotopic compositions, indicating that agpaitic rocks are derived from different mantle sources.

Acknowledgements

This work was supported by the Natural Science Foundation of China (grant 49634019) and Deutsche Forschungsgemeinschaft (grants Ma 2135/1–5, 4–2, 11–1, 11–2 and 12–1). Nelson Eby, Zhi-Li Qiu, Michele Lustrino, Katharina Pfaff and Julian Schilling are greatly appreciated for providing Lovozero (LV01–LV04), Khibiny (KB-0) and Poços de Caldas (PDC), Ilimaussaq and Mt. St. Hilaire samples. Wei-Qiang Ji is thanked for his assistance during sample preparation and analyses. Discussion with Yong-Fei Zheng benefits the calculation of Pb closure temperature. Constructive reviews by Bill Griffin and another anonymous referee improved the manuscript.

Appendix A. Sample descriptions

A.1. Ilímaussaq, Greenland

The Ilímaussaq complex, located in southwest Greenland, was emplaced at ~1160 Ma and cooled very rapidly (Waight et al., 2002; Upton et al., 2003; Krumrei et al., 2006). This complex was derived from three magma batches: an early augite syenite; an intermediate alkali granite; and later agpaitic syenites (Marks et al., 2004; Sørensen, 2006). The latter, which form the major part of the complex, are grouped into roof cumulates of sodalite foyaites and naujaites, floor cumulates of kakortokites and residual liquids of lujavrites. According to available data, the Ilímaussaq syenites exhibit a wide Sr–Nd isotopic variation (Blaxland et al., 1976; Paslick et al., 1993; Stevenson et al., 1997; Marks et al., 2004). As far as we are aware, only one sample of Ilímaussaq eudialyte has been analysed for its Hf isotopic composition with $^{176}Lu/^{177}Hf$ and $^{176}Hf/^{177}Hf$ values of 0.004595 and 0.282307 ± 21 (Patchett et al., 1981). If the new decay constant of ^{176}Lu ($1.87\times10-9\ y^{-1}$) and updated JMC475 $^{176}Hf/^{177}Hf$ value (0.282160) are accepted, the corrected $^{176}Hf/^{177}Hf$ and $\varepsilon_{Hf}(t)$ values are 0.282267 ± 21 and +4.3 ± 0.7, respectively. In addition, Waight et al. (2002) have reported a high $^{87}Sr/^{86}Sr$ isotopic ratio of 0.71149 ± 2 for eudialytes from this complex.

Samples GM1369 (60°58′6.13″N, 45°51′51.96″W, Fig. A1-a) and GM1370 (60°58′2.56″N, 45°52′53.77″W, Fig. A1-b) are naujaite from

Fig. A1. Representative images of eudialytes in the studied samples. (a) GM1370: subhedral eudialyte (Eud), associated with sodalite (Sod), aegirine (green) and arfvedsonite (black); (b) GM1369: BSE image of homogeneous eudialyte (black spots are laser pits); (c) KP21: two eudialyte phenocrysts set in a matrix of aligned aegirine (green), albite and microcline; (d) KP58: euhedral eudialyte associated with microcline (Mic) and needle-like aegirine (Aeg) (after Pfaff et al., 2008); (e) GM1335: euhedral eudialyte associated with interstitial arfvedsonite and K-feldspar (upper left); (f) ILM 101: euhedral, sector-zoned eudialyte crystals set in a fine-grained matrix of euhedral albite laths; (g) KB-0: pegmatitic syenite with purple eudialyte (g1), the eudialyte is subhedral and associated with aegirine (g2); (h) KB-1: subhedral eudialyte and associated aegirine (black); (i) KB-2: subhedral eudialyte with laser pits; (j) KB-3: a euhedral eudialyte crystal within matrix of apatite, aegirine and microcline; (k) LV13: euhedral eudialyte associated with aligned aegirine (dark green), phlogopite (brown) and altered K-feldsapr (k1), the eudialyte shows sector zoning; (l) LV01: large eudialyte grain (l1) with homogeneous internal structure (l2); (m) LV02: BSE image of eudialyte (with laser ablation pits); (n) LV03: BSE image of eudialyte (with laser ablation pits); (o) LV04: BSE image of eudialyte (with laser ablation pits); (p) SM06: euhedral eudialytes within a matrix of aegirine, altered nepheline and K-feldspar; (q) SM07: subhedral eudialyte associated with aegirine, altered nepheline, and K-feldspar; (r): SM25 (BSE image): a subhedral eudialyte crystal with marginal alteration; (s) TMZ 177: euhedral eudialytes with inclusions of aegirine needles; (t) TMZ241: subhedral eudialyte set in a matrix of aegirine needles (green) and albite laths; (u) TMZ298: subhedral eudialyte with euhedral inclusion of sodalite, associated with K-feldspar (upper part of the picture) and aegirine (dark green); (v) MSH 38: euhedral eudialyte associated with altered K-feldspar (lower right) and aegirine + arfvedsonite. (w) MSH 52: subhedral eudialyte in a matrix of partly-altered nepheline and K-feldspar associated with euhedral aegirine needles; (x) PDC: BSE image showing aegirine inclusions within eudialyte; and (y) KPW: pegmatitic eudialyte associated with black agrellite (y1). The eudialyte shows homogeneous internal structure in BSE images (y2) (with laser ablation pits); and (z) LGS: large eudialyte phenocryst surrounded by apatite, albite and aegirine (with laser ablation pits).

the roof sequence. They are coarse-grained and consist of sodalite, alkali feldspar, nepheline, amphibole, eudialyte and aegirine. Samples KP21 (60°52′57.35″N, 45°50′17.05″W, Fig. A1-c) and KP58 (60°53′48.61″N, 45°50′15.10″W, Fig. A1-d) are lujavrite from the middle sequence and consist of aegirine, nepheline, microcline, albite, eudialyte and analcime. Sample GM1335 (60°52′9.61″N, 45°51′

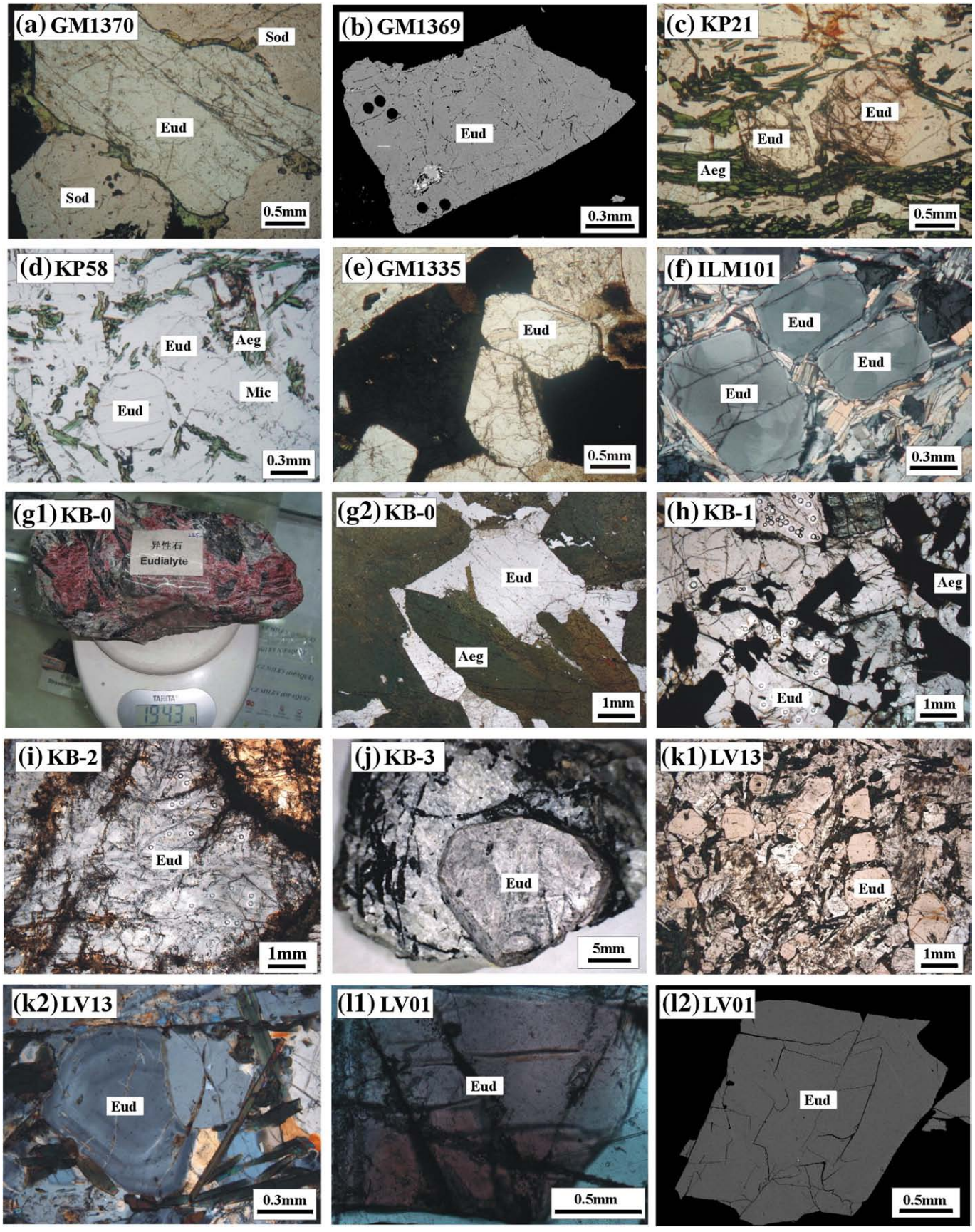

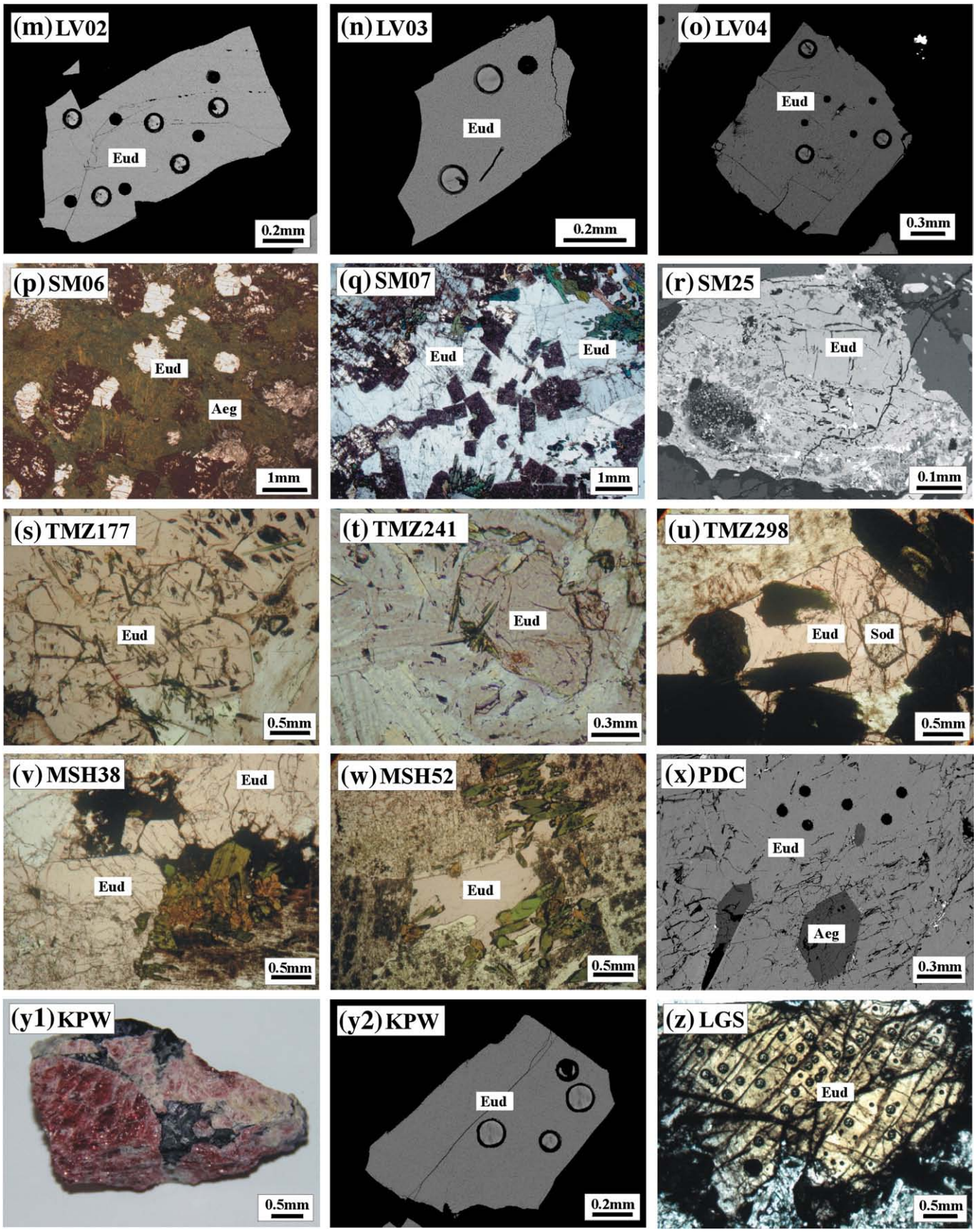

Fig. A1 (*continued*).

26.05″W) is a kakortkite from the floor sequence, and consists of eudialyte, feldspar, aenigmatite, natrolite and fluorite (Fig. A1-e). Sample ILM101 (60°52′33.27″N, 45°49′11.94″W, Fig. A1-f) is a late dyke of aplite. The detailed mineral compositions and petrology of these samples have been previously described (Markl et al., 2001; 2004, 2007; Pfaff et al., 2008).

A.2. Khibiny, Kola, Russia

Khibiny of the Kola Peninsula is the largest alkaline complexes in the world with an area of 1370 km^2 (Arzamastsev et al., 2001). The complex is mainly composed of agpaitic nepheline syenite, ultramafic (peridotite, pyroxenite and melilite-bearing) rocks, and minor carbonatite, in which the nepheline syenite is characterized by extensive occurrence of eudialyte (Arzamastsev et al., 2001, 2005). Available data indicate that this complex was emplaced during the Devonian time with age of ~358 to 388 Ma (Kramm et al., 1993; Kramm and Kogarko, 1994; Downes et al., 2005; Arzamastsev et al., 2007), if the Lu–Hf isochron age of 402.4 ± 2.8 Ma reported by Barfod et al. (2003) is excluded. It was shown that this complex has low initial Sr isotopic ratios of 0.7030–0.7043 with positive $\varepsilon_{Nd}(t)$ values of +1.3 to +6.0 (Kramm et al., 1993; Kramm and Kogarko, 1994; Downes et al., 2005). Patchett et al. (1981) reported an $^{176}Hf/^{177}Hf$ isotopic ratio of 0.282823 ± 18 for one sample of eudialyte from the complex, with $^{176}Lu/^{177}Hf$ value of 0.00163. If the new decay constant of ^{176}Lu and updated JMC475 $^{176}Hf/^{177}Hf$ ratio are accepted, the $^{176}Hf/^{177}Hf$ and $\varepsilon_{Hf}(t)$ values are 0.282783 ± 18 and 8.1 ± 0.6. Using a laser ablation technique, Barfod et al. (2003) obtained $^{176}Hf/^{177}Hf$ isotopic ratios of 0.282803 ± 7 and 0.282798 ± 15 ($\varepsilon_{Hf}(t)$ values of +9.0 ± 0.3 and +8.8 ± 0.5) for the eudialytes in the complex. Similarly, there are three recent studies of Hf isotopic measurements of eudialytes from this complex using laser ablation technique (Korgarko et al., 2008; Lahaye et al., 2008a,b; Kogarko et al., 2010). Although no detailed data are available, it is considered that the Khibiny has an average $\varepsilon_{Hf}(t)$ value of +8.0 ± 2.2.

Four samples were selected for analysis in this study. Samples KB-0, KB-1 and KB-2 were collected from the Vostochny open cast mine of Koashva in the Khibiny complex; and KB-3, provided by the Mineralogical Research Company, was collected from the apatite mineral pit at Mt. Rasvumchorr. KB-0 is a massive and laminated nepheline-bearing syenite with a weight of ~2 kg (Fig. A1-g1). It is partly pegmatitic with mineral grain-size of >5 mm. The constituent minerals include: eudialyte (~55%); aegirine (~45%); with minor amounts of agrellite, titanite, nepheline, albite and potash feldspar, etc. (Fig. A1-g2). Pale pinkish-gray pinacoidal eudialyte occurs as phenocrysts with a diameter of ~20 mm. Sample KB-1 is a coarse-grained nepheline syenite with a mineral assemblage of aegirine; arfvedsonite; nepheline; potash feldspar; and eudialyte (Fig. A1-h). Sample KB-2 is a pegmatite consisting of: aegirine; phlogopite; and eudialyte; with a grain-size of ~1 cm (Fig. A1-i). Sample of KB-3, consists of light greenish apatite, aegirine, microcline and eudialyte, and contains two large pinacoid crystals of eudialyte with grain-sizes of 22 × 22 × 6 and 20 × 18 × 9 mm^3. The latter crystal was chosen for analyses as it contains few inclusion of aegirine (Fig. A1-j).

A.3. Lovozero, Kola, Russia

Lovozero is the second largest alkaline complex in Kola Peninsula with an area of 650 km^2 (Arzamastsev et al., 2001). It is composed mainly of poikilitic feldspathoid syenite, layered lujavrite–foyaite–urtite and eudialyte nepheline syenite (lujavrite) with minor later alkaline volcanic rocks and dykes. Available data indicate that this complex was emplaced during the Devonian time with absolute age of ~347 to 372 Ma (Kramm et al., 1993; Kramm and Kogarko, 1994; Arzamastsev et al., 2007). It was also proposed that this complex had a rapid cooling history (Féménias et al., 2005). Isotopic analyses indicate that this complex is characterized by low initial Sr isotopic ratios of 0.7034–0.7040 and positive $\varepsilon_{Nd}(t)$ values of +2.9 to +4.9 (Kramm et al., 1993; Kramm and Kogarko, 1994; Downes et al., 2005). In recent studies, Hf isotopic measurements of eudialytes from this complex using laser ablation technique yield an average $\varepsilon_{Hf}(t)$ value of +6.4 ± 2.3 (Korgarko et al., 2008; Lahaye et al., 2008a,b).

Five samples were collected for this study. Sample LV13 is a coarse-grained melanocratic eudialyte-bearing lujavrite with strong planar lamination (Fig. A1-k1), consisting of alkali feldspar, nepheline, apatite, loparite and eudialyte, in which the euhedral eudialyte develops sector zoning (Fig. A1-k2). Samples LV01 (Fig. A1-l1), LV02 (Fig. A1-l2), LV03 (Fig. A1-m) and LV04 (Fig. A1-n) are large eudialyte crystals from pegamatitic lujavrite in the Alluaiv mining pit.

A.4. Saima, China

The ~230 Ma Saima complex is located in the Liaodong Peninsula of northern China. With an area of 280 km^2 (Chen and Saima Deposit Research Group, 1978; Chen, 1996), this complex is composed of an eastern syenite; central alkaline volcanic rocks (trachyte, leucite phonolite and syenitic porphyry); and western nepheline syenite (Jing et al., 1995; Chen, 1996; Zhou et al., 1996). The western coarse-grained eudialyte-bearing nepheline syenite is characterized by uranium mineralization, and consists of nepheline, potassium feldspar; biotite; aegirine; arfvedsonite; agrellite; eudialyte; and rare rinkolite and lamprophyllite. The eudialyte-enriched syenite typically shows mineral layering with eudialyte comprising up to 90 vol.% locally. The syenite has agpaitic ranging up to 1.5 (Chen, 1996; Tan et al., 1999). Whole-rock analyses give an initial Sr isotopic ratio of ~0.7060–0.7089 (Jing et al., 1995; Chen, 1996; Zhou et al., 1996). No Nd and Hf isotopic data are available for this complex to date.

Three samples (SM06, SM07 and SM25) from the Saima complex were selected for this in this study. These samples have similar mineral assemblages of nepheline, microcline, aegirine, eudialyte, titanite and biotite. Most eudialyte in these samples occur as idiomorphic crystals with grain-sizes up to 1 mm (Fig. A1-p and A1-q). However, some eudialyte from SM25 shows variable degrees of alteration (Fig. A1-r). Rarely, some eudialyte grains occur as pseudomorphs with complete replacement of eudialyte by secondary zircon, catapleiite, allanite, aegirine, nepheline, natrolite, titanite.

A.5. Tamazeght, Morocco

Tamazeght is a multiple plutonic-to-sub-volcanic complex located in the High Atlas mountains of Morocco, consisting of glimmerite, pyroxenite, shonkinite, gabbro, monzonite and nepheline syenite. The latter form the major component of the complex. The mineral assemblage of the nepheline syenite is nepheline; aegirine; alkali feldsar; eudialyte; titanite; and magnetite (Salvi et al., 2000; Marks et al., 2008a,b). U–Pb age determination of zircons from the monzonite and a late-stage hydrothermal vein yield indistinguishable ages of 44.5 ± 2.2 and 43.1 ± 1.8 Ma, and are taken as the emplacement age of the nepheline syenite (Marks et al., 2008b). The eudialyte samples investigated here are pegmatitic crystals from: a nepheline syenite (TMZ241, 32°31′80.74″N, 4°42′9.56″W, Fig. A1-s)), malignite (TMZ298, 32°31′13.32″N, 4°42′8.38″W, Fig. A1-t); and a late hydrothermal vein within malignite (TMZ177, 32°31′50.56″, N 4°42′55.56″ W, Fig. A1-u).

A.6. Mont Saint Hilaire, Quebec, Canada

Mont Saint Hilaire is part of the east–west trending Cretaceous anorogenic igneous Monteregian province of Quebec, which includes the Oka carbonatite. Mont Saint Hilaire is a mafic-alkaline intrusion composed of pyroxenite; gabbro; monzonite; and nepheline syenite (Currie et al., 1986). A perakaline syenite, characterized by a negative Eu anomaly forms the eastern part of the complex together with phonolite. Three analyses of whole-rock samples gave initial Sr isotopic values of 0.7037–0.7051

(Currie et al., 1986). Sample MSH38 (45°33′37.41″, N 73° 8′28.53″W, Fig. A1-v) and MSH52 (45°33′38.30″N, 73° 8′29.33″W, Fig. A1-w) in this study are coarse-grained (~5 mm) eudialytes from the nepheline syenite consisting of aegirine; Na-rich amphibole; nepheline; sodalite; ilmenite; magnetite, and eudialyte.

A.7. Poços de Caldas, Brazil

Poços de Caldas is the largest alkaline complex in South America with an area of ~800 km^2 (Schorscher and Shea, 1992), and is composed of peralkaline phonolite and nepheline syenite. The complex is subdivided into eudialyte-bearing and eudialyte-free syenites. It is generally accepted that the eudialyte-free nepheline syenite was formed at ~78 Ma, with initial Sr isotopic ratio of ~0.7051 and $\varepsilon_{Nd}(t)$ value of ~−3.5 (Shea, 1992). No previous data are available for the eudialyte-bearing nepheline syenites. Sample PDC, kindly provided by Michele Lustrino, was collected from the outcrop of Pedra Balao, a typical location for eudialyte in the north of the complex. The mineral is associated with nepheline; potassium feldspar; aegirine. The analysed eudialyte is pink in colour with grain-size of ~10 mm (Fig. A1-x).

A.8. Kipawa, Quebec, Canada

The sample KPW was collected from the Kipawa complex located in the Grenville province in Quebec of Canada. This complex, of nepheline syenite, amphibole syenite, quartz syenite and alkali granite, lies within gneiss as sheet-like body along the boundary between granitic and metasedimentary rocks (Currie and van Breemen, 1996). Geochronology suggests that the complex was emplaced ~1030 Ma ago, and underwent later metamorphism or genetically related to alkaline metasomatism from 1035 to 990 Ma (Currie and van Breemen, 1996; van Breemen and Currie, 2004). The eudialyte in this complex occurs in the late agpaitic pegmatites (Edgar and Black, 1972; Fryer and Edgar, 1977). The analysed sample is a mass of rose pink eudialyte with very minor dark purple veinlets of fluorite and minor agrellite. Eudialyte in this sample ranges from ~1 to 30 mm (Fig. A1-y).

A.9. Langesund Fjord, Norway

Langesunds Fjord is one of the well-known locations of eudialyte, which was traditionally named as eucolite (Bollingberg et al., 1983). The sample LGS is a medium-grained nepheline syenite collected at Arøy in Langesund Fjord, southeast of the Larvik complex; the latter being a part of the Permian Oslo alkaline province (Neuman, 1980). The eudialyte, occurred as phenocryst with grain-size of 1–5 mm, is associated with nepheline, aegirine, potassium feldspar, albite and apatite (Fig. A1-z).

References

Adams, C.J., Campbell, H.J., Griffin, W.L., 2005. Isotopic microanalysis of seawater strontium in biogenic calcite to assess subsequent rehomogenisation during metamorphism. Chemical Geology 220, 67–82.

Arzamastsev, A.A., Bea, F., Glaznev, V.N., Arzamastsev, L.V., Montero, P., 2001. Kola alkaline province in the Paleozoic: evaluation of primary mantle magma composition and magma generation conditions. Russian Journal of Earth Science 3, 1–32.

Arzamastsev, A.A., Bea, F., Arzamastsev, L.V., Montero, P., 2005. Trace elements in minerals of the Khibina Massif as indicators of mineral formation evolution: results of LA-ICP-MS study. Geochemistry International 43, 71–85.

Arzamastsev, A.A., Arzamastseva, L.V., Travin, A.V., Belyatsky, B.V., Shamatrina, A.M., Antonov, A.V., Larionov, A.N., Rodionov, N.V., Sergeev, S.A., 2007. Duration of formation of magmatic system of polyphase Paleozoic alkaline complexes of the Central Kola: U–Pb, Rb–Sr, Ar–Ar data. Doklady Earth Science 413A, 432–436.

Aulbach, S., O'Reilly, S.Y., Griffin, W.L., Pearson, N.J., 2008. Subcontinental lithospheric mantle origin of high niobium/tantalum ratios in eclogites. Nature Geosciences 1, 468–472.

Bailey, J.C., Gwozdz, R., Rose-Hansen, J., Sørensen, H., 2001. Geochemical overview of the Ilímaussaq alkaline complex, South Greenland. Geology of Greenland Survey Bulletin 190, 35–54.

Bailey, J.C., Sorensen, H., Andersen, T., Kogarko, L.N., Rose-Hansen, J., 2006. On the origin of microrhythmic layering in arfvedsonite lujavrite from the Ilímaussaq complex, South Greenland. Lithos 91, 301–318.

Barfod, G.H., Otero, O., Albarède, F., 2003. Phosphate Lu–Hf geochronology. Chemical Geology 200, 241–253.

Blaxland, A.B., van Breeman, O., Steenfelt, A., 1976. Age and origin of agpaitic magmatism at Ilímaussaq, south Greenland: Rb–Sr study. Lithos 9, 31–38.

Blichert-Toft, J., 2008. The Hf isotopic composition of zircon reference material 91500. Chemical Geology 253, 252–257.

Bollingberg, H.J., Ure, A.M., Sørensen, I., Leonardsen, E.S., 1983. Geochemistry of some eudialyte–eucolite specimens and a co-existing catapleiite from Langesund, Norway. TMPM Tschermaks Mineralogische und Petrolographische Mitteilungen 32, 153–169.

Chartier, F., Aubert, M., Salmon, M., Tabarant, M., Tran, B.H., 1999. Determination of erbium in nuclear fuels by isotope dilution thermal ionization mass spectrometry and glow discharge mass spectrometry. Journal of Analytical Atomic Spectrometry 14, 1461–1465.

Chen, Z.B., 1996. Saima Alkaline Complex and Mineralization. Atomic Energy Press, Beijing. 305 pp.

Chen, Z.B., Saima Deposit Research Group, 1978. Uranium deposit in the Saima alkaline massif, northeast China. Sciences in China 21, 365–389.

Choukroun, M., O'Reilly, S.Y., Griffin, W.L., Pearson, N.J., Dawson, J.B., 2005. Hf isotopes of MARID rutile trace metasomatic processes in the lithospheric mantle. Geology 33, 45–48.

Christensen, J.N., Halliday, A.N., Lee, D.C., Hall, C.M., 1995. *In situ* Sr isotopic analysis by laser ablation. Earth and Planetary Science Letters 136, 79–85.

Corfu, F., Dahlgren, S., 2008. Perovskite U–Pb ages and the Pb isotopic composition of alkaline volcanism initiating the Permo-Carboniferous Oslo rift. Earth and Planetary Science Letters 265, 256–269.

Coulson, I.M., 1997. Post-magmatic alteration in eudialyte from the North Qoroq centre, South Greenland. Mineralogical Magazine 61, 99–109.

Coulson, I.M., Chambers, A.D., 1996. Patterns of zonation in rare-earth-bearing minerals in nepheline sysnites of the North Qôroq center, South Greenland. Canadian Mineralogist 34, 1163–1178.

Cox, R.A., Wilton, D.H.C., 2006. U–Pb dating of perovskite by LA-ICP-MS: an example from the Oka carbonatite, Buebec, Canada. Chemical Geology 235, 21–32.

Currie, K.L., van Breemen, O., 1996. The origin of rare minerals in the Kipawa Syenite Complex, western Quebec. Canadian Mineralogist 34, 435–451.

Currie, K.L., Nelson, G.N., Gittins, J., 1986. The petrology of the Mont Saint Hilaire complex, southern Quebec: an alkaline gabbro-peralkaline syenite association. Lithos 19, 65–81.

Dahlgren, S., Corfu, F., Heaman, L.M., 1996. U–Pb isotopic time constraints, and Hf and Pb source characteristics of the Larvik plutonic complex, Oslo paleorift. Geodynamic and geochemical implications for the rift evolution. Journal of Conference Abstracts 1, 120.

Davidson, J.P., Morgan, D.J., Charlier, B.L.A., Harlou, R., Hora, J.M., 2007. Microsampling and isotopic analysis of igneous rocks: implications for the study of magmatic systems. Annual Review of Earth and Planetary Sciences 35, 273–311.

Dodson, M.H., 1973. Closure temperature in cooling geochronological and petrological systems. Contributions to Mineralogy and Petrology 40, 259–274.

Downes, H., Balaganskaya, E., Beard, A., Liferovich, R., Demaiffe, D., 2005. Petrogenetic processes in the ultramafic, alkaline and carbonatitic magmatism in the Kola alkaline province: a review. Lithos 85, 48–75.

Edgar, A.D., Black, C.E., 1972. Eudialyte from the Kipawa Lake area, Temiscamingue Co., Quebec. Canadian Mineralogist 11, 554–559.

Ehrlich, S., Gavrieli, I., Dor, L.B., Halicz, L., 2001. Direct high-precision measurements of the $^{87}Sr/^{86}Sr$ isotope ratio in natural water, carbonates and related materials by multiple collector inductively coupled plasma mass spectrometry (MC-ICP-MS). Journal of Analytical Atomic Spectrometry 16, 1389–1392.

Féménias, O., Coussaert, N., Brassinnes, S., Demaiffe, D., 2005. Emplacement processes and cooling history of layered cycle unit II-7 from the Lovozero alkaline massif (Kola Peninsula, Russia). Lithos 83, 371–393.

Fortunato, G., Mumic, K., Wunderli, S., Pillonel, L., Bosset, J.O., Gremand, G., 2004. Application of strontium isotope abundance ratios measured by MC-ICP-MS for food authentication. Journal of Analytical Atomic Spectrometry 19, 227–234.

Foster, G.L., Vance, D., 2006. *In situ* Nd isotopic analysis of geological materials by laser ablation MC-ICP-MS. Journal of Analytical Atomic Spectrometry 21, 288–296.

Frost, B.R., Chamberlain, K.R., Schumacher, J.C., 2000. Sphene (titanite): phase relations and role as a geochronometer. Chemical Geology 172, 131–148.

Fryer, B.J., Edgar, A.D., 1977. Significance of rare earth distributions in coexisting minerals of peralkaline undersaturated rocks. Contributions to Mineralogy and Petrology 61, 35–48.

Gregory, C.J., McFarlane, C.R.M., Hermann, J., Rubatto, D., 2009. Tracing the evolution of calc-alkaline magmas: in-situ Sm–Nd isotope studies of accessory minerals in the Bergell igneous complex, Italy. Chemical Geology 260, 73–86.

Griffin, W.L., Pearson, N.J., Belousova, E., Jackson, S.E., van Achterbergh, E., O'Reilly, S.Y., Shee, S.R., 2000. The Hf isotope composition of cratonic mantle: LAM-MC-ICPMS analysis of zircon megacrysts in kimberlites. Geochimica et. Cosmochimica Acta 64, 133–147.

Griffin, W.L., Powell, W.J., Pearson, N.J., O'Reilly, S.Y., 2008. GLITTER: data reduction software for laser ablation ICP-MS. In: Sylvester, P. (Ed.), Laser Ablation-ICP-MS in the Earth Sciences: Current Practices and Outstanding Issues: Mineralogical Association of Canada Short Course, vol. 40, pp. 308–311.

Jing, L.Z., Guo, Y.J., Ding, C.X., 1995. Geochronology and origin of the Saima alkaline rocks in Liaoning Province (in Chinese with English abstract). Liaoning Geology 4, 257–271.

Johnsen, O., Gault, R.A., 1997. Chemical variation in eudialyte. Neues Jahrbuch für Mineralogie Abhandlungen 171, 215–237.

Johnsen, O., Ferraris, G., Gault, R.A., Grice, J.D., Kampf, A.R., Pekov, I.V., 2003. The nomenclature of eudialyte-group minerals. Canadian Mineralogist 41, 785–794.

Kogarko, L.N., Lazutkina, L.N., Romanchev, B.P., 1982. The origin of eudialyte mineralization. Geochemistry International 19 (5), 128–145.
Kogarko, L.N., Lahaye, Y., Brey, G.P., 2010. Plume-related mantle source of super-large rare metal deposits from the Lovozero and Khibina massifs on the Kola Peninsula, Eastern part of Baltic Shield: Sr, Nd and Hf isotope systematics. Minerology and Petrology 98, 197–208.
Korgarko, L.N., Lahaye, Y., Brey, G., 2008. Depleted mantle source of super-large rare metal deposits from the Kola Peninsula (first data on the Lu–Hf system). 33rd International Geological Congress, Abstract of 1259919.
Kramm, U., Kogarko, L.N., 1994. Nd and Sr isotope signatures of the Khibina and Lovozero agpaitic centres, Kola alkaline province, Russia. Lithos 32, 225–242.
Kramm, U., Kogarko, L.N., Kononova, V.A., Vartiainen, H., 1993. The Kola alkaline province of the CIS and Finland: precise Rb–Sr ages define 380–360 age range for all magmatism. Lithos 30, 33–44.
Krumrei, T.V., Villa, I.M., Marks, M., Markl, G., 2006. A $^{40}Ar/^{39}Ar$ and U/Pb isotopic study of the Ilímaussaq complex, South Greenland: implications for the ^{40}K decay constant and for the duration of magmatic activity in a peralkaline complex. Chemical Geology 227, 258–273.
Lahaye, Y., Kogarko, L.N., Grey, G.P., 2008a. Isotopic (Sr, Nd, Hf) composition of super-large metal deposits from the Kola Peninsula using in-situ LA-MC-CPMS. Geochimica et Cosmochimica Acta 72, A511.
Lahaye, Y., Kogarko, L.N., Grey, G.P., 2008b. Isotopic (Nd, Hf, Sr) composition of super-large rare metal deposits from the Kola Peninsula using in-situ LA-MC-ICPMS. 9th International Kimberlite Conference, Extended abstract of 00395.
Larsen, B.T., Olaussen, S., Sundvoll, B., Heeremans, M., 2008. The Permo-Carboniferous Oslo rift through six stages and 65 million years. Episodes 31, 52–58.
Ludwig, K.R., 2003. ISOPLOT 3.0—a geochronological toolkit for Microsoft Excel. Berkeley Geochronology Center Special Publication, No. 4. 70 pp.
Markl, G., Marks, M., Schwinn, G., Sommer, H., 2001. Phase equilibrium constraints on intensive crystallization parameters of the Ilímaussaq Complex, South Greenland. Journal of Petrology 42, 2231–2258.
Marks, M., Vennemann, T., Siebel, W., Markl, G., 2004. Nd-, O-, and H-isotopic evidence for complex, closed-system fluid evolution of the peralkaline Ilímaussaq Intrusion, South Greenland. Geochimica et. Cosmochimica Acta 68, 3379–3395.
Marks, M.A.W., Rudnick, R.L., McCammon, C., Vennemann, T., Markl, G., 2007. Arrested kinetic Li isotope fractionation at the margin of the Ilímaussaq complex, South Greenland: evidence for open-system processes during final cooling of peralkaline igneous rocks. Chemical Geology 246, 207–230.
Marks, M.A.W., Schilling, J., Coulson, I.M., Wenzel, T., Markl, G., 2008a. The alkaline–peralkaline Tamazeght complex, High Atlas Mountains, Morocco: mineral chemistry and petrological constraints for derivation from a compositionally heterogeneous mantle source. Journal of Petrology 49, 1097–1131.
Marks, M.A.W., Coulson, I.M., Schilling, J., Jacob, D.E., Schmitt, A.K., Markl, G., 2008b. The effect of titanite and other HFSE-rich mineral (Ti-bearing andradite, zircon, eudialyte) fractionation on the geochemical evolution of silicate melts. Chemical Geology 257, 153–172.
Marks, M.A.W., Neukirechen, F., Vennemann, T., Markl, G., 2009. Textural, chemical, and isotopic effects of late-magmatic carbonatitic fluids in the carbonatite–syenite Tamazeght complex, High Atlas Mountains, Morocco. Mineralogy and Petrology 97, 23–42.
McFarlane, C.R.M., McCulloch, M.T., 2007. Coupling of in-situ Sm–Nd systematics and U–Pb dating of monazite and allanite with applications to crustal evolution studies. Chemical Geology 245, 45–60.
McFarlane, C.R.M., McCulloch, M.T., 2008. Sm–Nd and Sr isotope systematics in LREE-rich accessory minerals using LA-ICP-MS. Mineralogical Association of Canada Short Course Series 40, 117–133.
Mitchell, R.H., Liferovich, R.P., 2006. Subsolidus deuteric/hydrothermal alteration of eudialyte in lujavrite from the Pilansberg alkaline complex, South Africa. Lithos 91, 352–372.
Münker, C., Weyer, S., Scherer, E.E., Mezger, K., 2001. Separation of high field strength elements (Nb, Ta, Zr, Hf) and Lu from rock samples for MC-ICPMS measurements. Geochemistry, Geophysics, Geosystems (G^3) 2, 10.1029. doi:10.1029/2001GC000183.
Neuman, E.R., 1980. Petrogenesis of the Oslo region larvikites and associated rocks. Journal of Petrology 21, 499–531.
Neumann, E.R., Tilton, G.R., Tuen, E., 1988. Sr, Nd and Pb isotope geochemistry of the Oslo rift igneous province, southeast Norway. Geochimica et Cosmochimica Acta 52, 1997–2007.
Olivo, G.R., Williams-Jones, A.E., 1999. Hydrothermal REE-rich eudialyte from the Pilansberg complex, South Africa. Canadian Mineralogist 37, 653–663.
Paslick, C.R., Halliday, A.N., Davies, G.R., Mezger, K., Upton, B.G.J., 1993. Timing of Proterozoic magmatism in the Gardar Province, southern Greenland. Geological Society of American Bulletin 105, 272–278.
Patchett, P.J., Kouvo, O., Hedge, C.E., Tatsumoto, M., 1981. Evolution of continental crust and mantle heterogeneity: evidence from Hf isotopes. Contributions to Mineralogy and Petrology 78, 279–297.
Paton, C., Hergt, J.M., Phillips, D., Woodhead, J.D., Shee, S.R., 2007a. New insights into the genesis of Indian kimberlites from the Dharwar Craton via *in situ* Sr isotope analysis of groundmass perovskite. Geology 35, 1011–1014.
Paton, C., Woodhead, J., Hergt, J., Phillips, D., Shee, S., 2007b. Sr-isotope analysis of kimberlitic groundmass perovskite via LA-MCICPMS. Geostandards and Geoanalytical Research 31, 321–330.
Pfaff, K., Krumrei, T., Marks, M.A.W., Wenzel, T., Rudolf, T., Markl, G., 2008. Chemical and physical evolution of the "lower layered sequence" from the nepheline syenitic Ilímaussaq intrusion, south Greenland: implications for the origin of magmatic layering in peralkaline felsic liquids. Lithos 106, 280–296.
Pin, C., Zalduegui, J.F.S., 1997. Sequential separation of light rare-earth elements, thorium and uranium by miniaturized extraction chromatography: application to isotopic analyses of silicate rocks. Analytica Chimica Acta 339, 79–89.
Ramos, F.C., Wolff, J.A., Tollstrup, D.L., 2004. Measuring $^{87}Sr/^{86}Sr$ variation in minerals and groundmass from basalts using LA-MC-ICPMS. Chemical Geology 211, 135–158.
Rasmussen, E., Neumann, E.R., Andersen, T., Sundvoll, B., Fjerdingstad, V., Stabel, A., 1988. Petrogenetic processes associated with intermediate and silicic magmatism in the Olso rift, south-east Norway. Mineralogical Magazine 52, 293–307.
Salvi, S., Fontan, F., Monchoux, P., 2000. Hydrothermal mobilization of high field strength elements in alkaline igneous systems: evidence from the Tamazeght Complex, (Morocco). Economic Geology 95, 559–576.
Schilling, J., Marks, M.A.W., Wenzel, T., Markl, G., 2009. Reconstruction of magmatic to subsolidus processes in an agpaitic system using eudialyte textures and composition: a case study from Tamazeght, Morocco. Canadian Mineralogist 47, 351–365.
Schorscher, H.D., Shea, M.E., 1992. The regional geology of the Poços de Caldas alkaline complex: mineralogy and geochemistry of selected nepheline syenites and phonolites. Journal of Geochemical Exploration 45, 25–51.
Shea, M.E., 1992. Isotopic geochemical characterization of selected nepheline syenites and phonolites from the Poços de Caldas alkaline complex, Minas Gerais, Brazil. Journal of Geochemical Exploration 45, 173–214.
Sørensen, H., 1997. The agpaitic rocks—an overview. Mineralogical Magazine 61, 485–498.
Sørensen, H., 2006. The Ilímaussaq alkaline complex, south Greenland—an overview of 200 years of research and an outlook. Meddelelser om Grønland Geosciience 45, 1–70.
Sørensen, H., Bohse, H., Bailey, J.C., 2006. The origin and mode of emplacement of lujavrites in the Ilímaussaq alkaline complex, south Grenland. Lithos 91, 286–300.
Stacey, J.S., Kramers, J.D., 1975. Approximation of terrestrial lead isotope evolution by a two stages model. Earth and Planetary Science Letters 26, 207–221.
Stevenson, R., Upton, B.G.J., Steenfelt, A., 1997. Crust–mantle interaction in the evolution of the Ilímaussaq Complex, South Greenland: Nd isotopic studies. Lithos 40, 189–202.
Tan, D.J., Lin, J.Q., Shan, X.L., 1999. On magma origin of the Saima–Bolinchuan alkaline volcanic-intrusive complex (in Chinese with English abstract). Geological Review 45, 474–481 (supplement).
Thirlwall, M.F., Walder, A.J., 1995. *In situ* hafnium isotope ratio analysis of zircon by inductively coupled plasma multiple collector mass spectrometry. Chemical Geology 122, 241–247.
Upton, B.G.J., Emeleus, C.H., Heaman, L.M., Goodenough, K.M., Finch, A.A., 2003. Magmatism of the mid-Proterozoic Gardar Province, South Greenland: chronology, petrogenesis and geological setting. Lithos 68, 43–65.
van Breemen, O., Currie, K.L., 2004. Petrology and U–Pb geochronology of the Kipawa syenite complex—a thrust related alkaline pluton—and adjacent rocks in the Grenville province of western Quebec. Canadian Journal of Earth Sciences 41, 431–455.
Vervoort, J.D., Patchett, P.J., Soderlund, U., Baker, M., 2004. Isotopic composition of Yb and the determination of Lu concentrations and Lu/Hf ratios by isotopic dilution using MC-ICPMS. Geochemistry, Geophysics, Geosystems (G^3) 5, Q11002. doi:10.1029/2004GC000721.
Vroon, P.Z., van der Wagt, B., Koornneef, J.M., Davies, G.R., 2008. Problems in obtaining precise and accurate Sr isotope analysis from geological materials using laser ablation MC-ICPMS. Analytical and Bioanalytical Chemistry 390, 465–476.
Waight, T., Baker, J., Willigers, B., 2002. Rb isotope dilution analyses by MC–ICPMS using Zr to correct for mass fractionation: towards improved Rb–Sr geochronology? Chemical Geology 186, 99–116.
Weis, D., Kieffer, B., Maerschalk, C., Pretorius, W., Barling, J., 2005. High-precision Pb–Sr–Nd–Hf isotopic characterization of USGS BHVO-1 and BHVO-2 reference materials. Geochemistry, Geophysics, Geosystems (G^3) 6, Q02002. doi:10.1029/2004GC000852.
Weis, D., Kieffer, B., Maerschalk, C., Barling, J., Jong, J.D., Williams, G.A., Hanano, D., Pretorius, W., Mattielli, N., Scoates, J.S., Goolaerts, A., Friedman, R.M., Mahoney, J.B., 2006. High-precision isotopic characterization of USGS reference materials by TIMS and MC-ICP-MS. Geochemistry, Geophysics, Geosystems (G^3) 7, Q08006. doi:10.1029/2006GC001283.
Weis, D., Kieffer, B., Hanano, D., Nobre, Silva, I., Barling, J., Pretorius, W., Maerschalk, C., Mattielli, N., 2007. Hf isotope compositions of U.S. Geological Survey reference materials. Geochemistry, Geophysics, Geosystems (G^3) 8, Q06006. doi:10.1029/2006GC001473.
Wiedenbeck, M., Alle, P., Corfu, F., Griffin, W.L., Meier, F., Oberli, F., Von Quadt, A., Roddick, J.C., Spiegel, W., 1995. Three natural zircon standards for U–Th–Pb, Lu–Hf, trace element, and REE analyses. Geostandards Newsletters 19, 1–23.
Williams, I.S., 1998. U–Th–Pb geochronology by ion microprobe. In: McKibben, M.A., Shanks III, W.C., Ridley, W.I. (Eds.), Applications of Microanalytical Techniques to Understanding Mineralizing Processes: Reviews in Economic Geology, vol. 7, pp. 1–35.
Woodhead, J., Hergt, J., Shelley, M., Eggins, S., Kemp, R., 2004. Zircon Hf-isotope analysis with an excimer laser, depth profiling, ablation of complex geometries, and concomitant age estimation. Chemical Geology 209, 121–135.
Woodhead, J., Swearer, S., Hergt, J., Maas, R., 2005. *In situ* Sr-isotope analysis of carbonates by LA-MC-ICP-MS: interference corrections, high spatial resolution and an example from otolith studies. Journal of Analytical Atomic Spectrometry 20, 22–27.
Wu, F.Y., Yang, Y.H., Xie, L.W., Yang, J.H., Xu, P., 2006. Hf isotopic compositions of the standard zircons and baddeleyites used in U–Pb geochronology. Chemical Geology 234, 105–126.
Wu, F.Y., Yang, Y.H., Mitchell, R.H., Zhang, Y.B., 2010. *In situ* U–Pb age determination and Nd isotopic analyses of perovskites from kimberlites in southern Africa and Somerset Island, Canada. Lithos 115, 205–222.
Xie, L.W., Zhang, Y.B., Zhang, H.H., Sun, J.F., Wu, F.Y., 2008. *In situ* simultaneous determination of trace elements, U–Pb and Lu–Hf isotopes in zircon and baddeleyite. Chinese Science Bulletin 53, 1565–1573.

Yang, Y.H., Zhang, H.F., Xie, L.W., Wu, F.Y., 2007. Accurate measurement of neodymium isotopic composition using Neptune multiple collector inductively coupled plasma mass spectrometry (in Chinese with English abstract). Chinese Journal of Analytical Chemistry 35, 71–74.

Yang, Y.H., Sun, J.F., Xie, L.W., Fan, H.R., Wu, F.Y., 2008. *In situ* Nd isotopic measurement of geological samples by laser ablation. Chinese Science Bulletin 53, 1062–1070.

Yang, Y.H., Wu, F.Y., Wilde, S.A., Liu, X.M., Zhang, Y.B., Xie, L.W., Yang, J.H., 2009. *In situ* perovskite Sr–Nd isotopic constraints on petrogenesis of the Mengyin kimberlites in the North China Craton. Chemical Geology 264, 24–42.

Yang, Y.H., Zhang, H.F., Chu, Z.Y., Xie, L.W., Wu, F.Y., 2010. Combined chemical separation of Lu, Hf, Rb, Sr, Sm and Nd from a single rock digest and precise and accurate isotope determinations of Lu–Hf, Rb–Sr and Sm–Nd isotope systematics using multi-collector ICP-MS and TIMS. International Journal of Mass Spectrometry 290, 120–126.

Zhao, Z.F., Zheng, Y.F., 2007. Diffusion compensation for argon, hydrogen, lead, and strontium in minerals: empirical relationships to crystal chemistry. American Mineralogist 92, 289–308.

Zhou, L.D., Zhao, Z.H., Zhou, G.F., 1996. Isotopic chronology of some alkaline rocks bodies in China (in Chinese with English abstract). Geochimica 25, 164–171.